Title: mTORC1 and mTORC2 regulate distinct aspects of glutamatergic synaptic transmission.

Abbreviated Title: mTORC1 and mTORC2 regulation of synaptic transmission.

Matthew P. McCabe[1], Erin R. Cullen[1], Caitlynn M. Barrows[1], Amy N. Shore[1], Katharine I. Tooke[1], and Matthew C. Weston[1]

1. University of Vermont, Department of Neurological Sciences, Burlington, VT 05405.

Corresponding Author:
Matthew C. Weston
Department of Neurological Sciences
University of Vermont
95 Carrigan Dr.
Burlington, VT 05405
Email: mcweston@uvm.edu

Conflict of Interest: The authors declare no competing financial interests.

Acknowledgements: This work was supported by NIH/NINDS grants NS087095 and NS110945, and the COBRE Neuroscience award P30 103498. We thank Todd Clason, and the Molecular and Imaging Cores, at the University of Vermont. Thanks to John Clements for providing the deconvolution algorithm used to estimate the rate of synaptic vesicle release.

Abstract

Although mTOR signaling is known as a broad regulator of cell growth and proliferation, in neurons it regulates synaptic transmission, which is thought to be a major mechanism through which altered mTOR signaling leads to neurological disease. Although previous studies have delineated postsynaptic roles for mTOR, whether it regulates presynaptic function is largely unknown. Moreover, the mTOR kinase operates in two complexes, mTORC1 and mTORC2, suggesting that mTOR's role in synaptic transmission may be complex-specific. To better understand each complex's role in synaptic transmission, we genetically inactivated mTORC1 or mTORC2 in cultured mouse glutamatergic hippocampal neurons. Inactivation of either complex reduced neuron growth and evoked EPSCs, however, mTORC1 exerted its effects on eEPSCs at the postsynapse and mTORC2 at the presynapse. Furthermore, inactivation of each complex altered specific modes of synaptic vesicle release, suggesting that mTORC1 and mTORC2 differentially modulate postsynaptic responsiveness and presynaptic release to optimize glutamatergic synaptic transmission.

Introduction

The mechanistic target of rapamycin (mTOR) signaling network is an evolutionarily conserved group of interacting proteins centered around the ubiquitously expressed serine/threonine kinase mTOR. In a variety of species and cell types, mTOR signaling regulates fundamental cell biological processes such as cell growth, survival, and division (Saxton & Sabatini, 2017). In the nervous system, however, mTOR signaling plays a more specific role in neuronal communication by tuning the strength of synaptic connections (Henry et al., 2012; Huang et al., 2013; Niere et al., 2016; Sperow et al., 2012; Weston, Chen, & Swann, 2014). This regulation of synaptic strength by mTOR is thought to be necessary for learning and memory, setting E-I balance, and maintaining synaptic homeostasis. Furthermore, variants in several genes in the mTOR signaling network cause neurological diseases including epilepsy and autism (Crino, 2011; Lipton & Sahin, 2014), and increasing evidence suggests that dysregulation of synaptic transmission is a key feature of these diseases (Zoghbi & Bear, 2012).

A broad distinction in the organization of the mTOR signaling network is that the mTOR kinase operates in two multiprotein complexes, mTORC1 and mTORC2 (Hay & Sonenberg, 2004). Both the substrates of mTOR and the downstream cellular processes it affects are different depending on its association with mTORC1 or mTORC2 (Wullschleger, Loewith, & Hall, 2006). Biochemically, mTORC1 and mTORC2 are distinguished by their protein composition. Although they both contain mTOR and other components such as Deptor and mLST8, Raptor is a protein that is unique to mTORC1 and is essential to its function, whereas Rictor is unique to mTORC2 and essential to its function. Pharmacologically, the mTOR inhibitor rapamycin and its derivatives are more effective at inhibiting mTORC1 than mTORC2 (Kang et al., 2013), but this distinction is lessened with longer exposure and at higher concentrations (Sarbassov et al., 2006).

Previous studies have demonstrated changes in postsynaptic function by manipulating mTOR signaling either pharmacologically or genetically. Because of the link between mTOR, protein synthesis,

and long-term synaptic plasticity, several studies have shown the necessity for intact mTORC1 and mTORC2 function in long-term potentiation and long-term depression (Huang et al., 2013; Stoica et al., 2011; S. J. Tang et al., 2002). At the molecular level, mTOR signaling and its downstream targets are known to regulate AMPA receptor expression and synapse number (Ran et al., 2013; Wang, Barbaro, & Baraban, 2006). More recently, postsynaptic loss of mTORC1 was shown to reduce evoked excitatory postsynaptic current (eEPSC) amplitudes onto Purkinje neurons, but mTORC2 loss did not, suggesting specific roles for the two complexes in the regulation of synaptic transmission (Angliker, Burri, Zaichuk, Fritschy, & Ruegg, 2015).

Despite progress in delineating the regulation of postsynaptic function by mTOR, the role of mTOR in presynaptic function, and more specifically synaptic vesicle (SV) release, is largely unexplored. Studies at the *Drosophila* neuromuscular junction and in rat hippocampal neurons have shown that postsynaptic mTORC1 activity provides a retrograde signal that enhances the readily releasable pool (RRP) of SVs in response to a reduction in postsynaptic glutamate receptor activity (Henry et al., 2012; Henry et al., 2018; Penney et al., 2012), and another study found that a high dose of rapamycin (3 µm) depleted dopaminergic SVs from presynaptic terminals in the striatum (Hernandez et al., 2012), but none of these studies examined SV release itself. Interestingly, several recent studies have uncovered roles for IGF-1 receptor signaling, protein synthesis, and cholesterol biosynthesis in regulating the balance of spontaneous and evoked SV release (Gazit et al., 2016; Scarnati, Kataria, Biswas, & Paradiso, 2018; Wasser, Ertunc, Liu, & Kavalali, 2007). Because these processes are up- and downstream of mTOR, this raises the possibility that mTOR may act as a hub to regulate different modes of SV fusion.

To assess the pre- and postsynaptic function of each mTOR complex in glutamatergic synaptic transmission, we inactivated mTORC1 signaling by conditionally deleting *Raptor*, or mTORC2 signaling by conditionally deleting *Rictor,* postmitotically in primary neuron cultures from mouse hippocampus. We then performed morphological and whole-cell patch-clamp analysis of synaptic and membrane

properties of glutamatergic neurons. Our results showed that both mTOR complexes are necessary to support normal neuron growth and evoked excitatory synaptic transmission, although the effects of mTORC1 on eEPSCs are postsynaptic and mTORC2 presynaptic. We further showed that each mTOR complex affects distinct modes of SV release: mTORC1 inactivation enhances modes with low rates of SV fusion, such as spontaneous release, and mTORC2 inactivation impairs modes with high rates of SV fusion, such as action potential-evoked release. Thus, mTORC1 and mTORC2 operate at distinct synaptic locations and in distinct processes, and via differential activation of these two complexes, the mTOR pathway is ideally poised to respond to external cues and make fine adjustments to glutamatergic synaptic transmission to maintain normal neural network function.

Results

Inactivation of mTORC1 or mTORC2 in neurons, via *Raptor* or *Rictor* deletion, causes distinct effects on downstream mTOR signaling.

To investigate the effects of mTORC1 or mTORC2 inactivation on neurons, we cultured primary hippocampal neurons isolated from P0-P1 *Raptor*$^{flox/flox}$ or *Rictor*$^{flox/flox}$ mice on astrocytes isolated from P0-P1 wild-type mice. At the time of plating, we transduced the neurons with adeno-associated viruses (AAVs) expressing either an mCherry-Cre fusion protein or mCherry alone, both driven by the hSyn promoter, to generate knockout (Raptor-KO or Rictor-KO) or control (Raptor-Con or Rictor-Con) neurons, respectively. To assess the efficiency of gene deletion in Raptor-KO and Rictor-KO neurons, we performed quantitative immunofluorescence analysis for phospho-S6 (S240/244) (pS6), an indicator of mTORC1 activity, and phospho-Akt (S473) (pAkt), an indicator of mTORC2 activity. In Raptor-KO neurons, the mean fluorescence intensity of the pS6 signal was decreased relative to Raptor-Con neurons (Con: 1.00 ± 0.05, Rap-KO: 0.25 ± 0.03, $p < 0.001$; Figure 1A$_{1-3}$), verifying a reduction in mTORC1 activity. The pAkt signal was, however, increased in Raptor-KO neurons relative to Raptor-Con neurons (Con: 1.00 ±

0.05, Rap-KO: 1.31 ± 0.06, $p < 0.001$; Figure 1B_{1-3}), likely due to release of the negative feedback loop from mTORC1 to insulin receptor signaling (Hsu et al., 2011; O'Reilly et al., 2006). Rictor-KO neurons showed reduced levels of pAkt immunofluorescence relative to Rictor-Con neurons (Con: 1.00 ± 0.03, Ric-KO: 0.56 ± 0.02, $p < 0.001$; Figure 1E_{1-3}), as expected because the S473 residue on Akt is a known target of mTORC2. pS6 levels were also reduced in Rictor-KO neurons compared with those of Rictor-Con neurons (Con: 1.00 ± 0.05, Ric-KO: 0.55 ± 0.03, $p < 0.001$; Figure 1F_{1-3}), likely because reduced Akt phosphorylation dampens signaling through the Akt-Tsc-mTORC1 axis. Thus, Cre expression in *Raptor*$^{flox/flox}$ and *Rictor*$^{flox/flox}$ neurons causes distinct biochemical changes consistent with reductions in mTORC1 and mTORC2 activity, respectively.

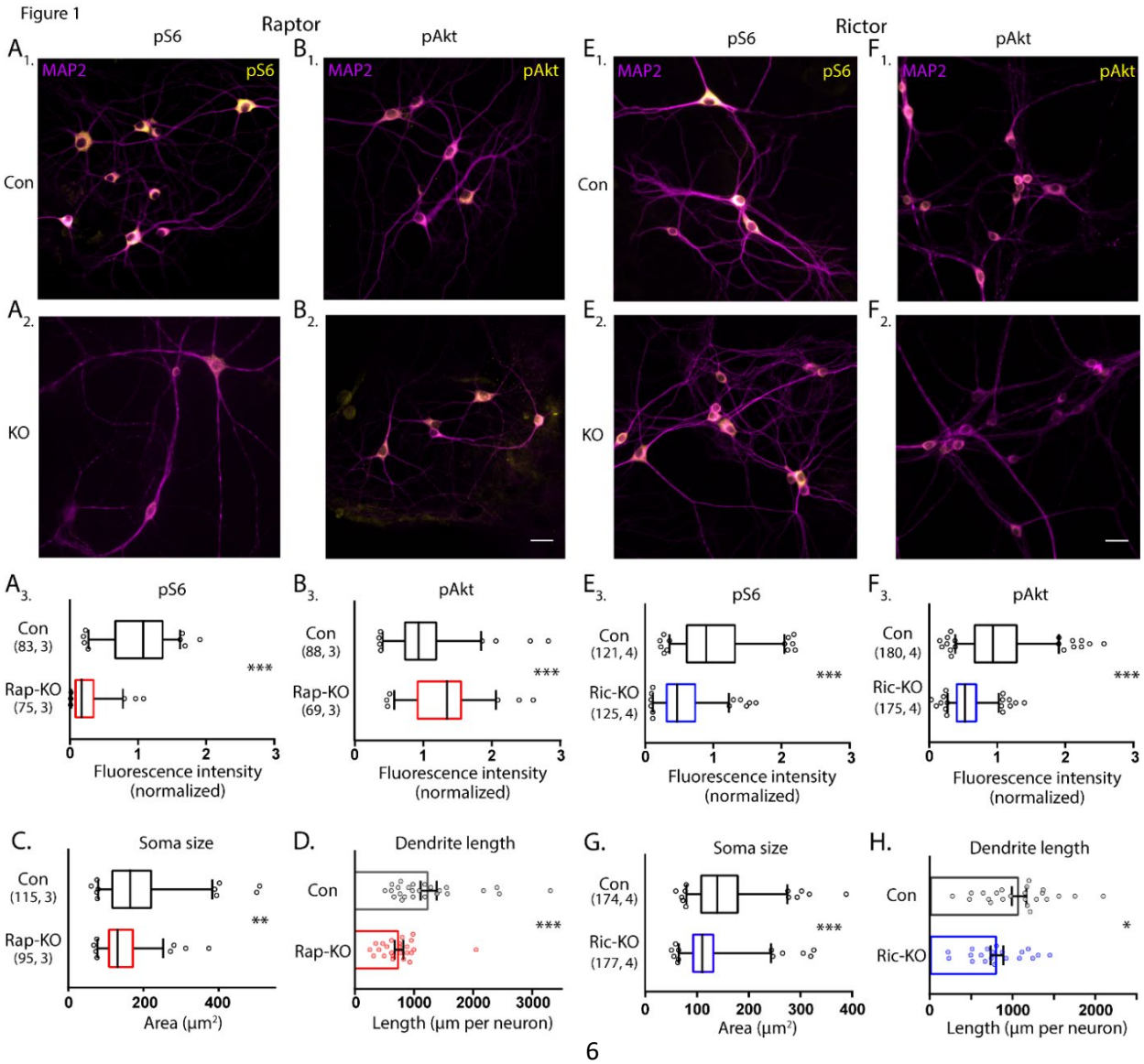

Figure 1. Loss of Raptor or Rictor in primary hippocampal neurons alters mTOR signaling and decreases neuron growth. A. Representative images of Raptor-Con (A_1) and Raptor-KO neurons (A_2) showing the structure of the neurons revealed by MAP2 immunofluorescence (purple) and the immunofluorescence signal from phospho-S6 (pS6, yellow) A_3. Box plot (median and 95%) showing the fluorescence intensity measurements from the pS6 signal in Raptor-Con and Raptor-KO neurons. B. Representative images of Raptor-Con (B_1) and Raptor-KO neurons (B_2) showing the structure of the neurons revealed by MAP2 immunofluorescence (purple) and the immunofluorescence signal from phospho-AKT_{473} (pAkt, yellow) Scale bar is 25 µm. B_3. Box plot (median and 95%) showing the fluorescence intensity measurements from the pAkt signal in Raptor-Con and Raptor-KO neurons. C. Box plot (median and 95%) showing the area measurements of the somatic compartment in Raptor-Con and Raptor-KO neurons. D. Dot plot showing the measurements of the total dendritic length in Raptor-Con and Raptor-KO neurons and mean ± s.e.m. E. Representative images of Rictor-Con (E_1) and Rictor-KO neurons (E_2) showing the structure of the neurons revealed by MAP2 immunofluorescence (purple) and the immunofluorescence signal from phospho-S6 (pS6, yellow) E_3. Box plot (median and 95%) showing the fluorescence intensity measurements from the pS6 signal in Rictor-Con and Rictor-KO neurons. F. Representative images of Rictor-Con (F_1) and Rictor-KO neurons (F_2) showing the structure of the neurons revealed by MAP2 immunofluorescence (purple) and the immunofluorescence signal from phospho-AKT_{473} (pAkt, yellow) Scale bar is 25 µm. F_3. Box plot (median and 95%) showing the fluorescence intensity measurements from the pAkt signal in Rictor-Con and Rictor-KO neurons. G. Box plot (median and 95%) showing the area measurements of the somatic compartment in Rictor-Con and Rictor-KO neurons. H. Dot plot showing the measurements of the total dendritic length in Rictor-Con and Rictor-KO neurons and mean ± s.e.m. The numbers underneath the groups indicate the number of neurons analyzed and the number of cultures. * = $p < 0.05$, ** = $p < 0.01$, *** = $p < 0.001$, as tested with Generalized Estimating Equations.

Raptor or Rictor loss results in similar effects on neuron morphology and passive membrane properties.

In addition to biochemical markers, mTOR signaling is known to regulate cell size (Edinger & Thompson, 2002; D. H. Kim et al., 2002; Urbanska, Gozdz, Swiech, & Jaworski, 2012); in particular, dramatic increases in cell size occur in most cell types following hyperactivation of the mTOR pathway. To assess alterations in neuron size, we measured neuronal soma area in the cultures following deletion of *Raptor* and *Rictor*. For Raptor-KO and Rictor-KO neurons, soma areas were reduced by almost 20% compared with those of their respective controls (Con: 180 ± 8 μm^2, Rap-KO: 146 ± 6 μm^2, $p = 0.007$; Con: 151 ± 5 μm^2, Ric-KO: 126 ± 4 μm^2, $p < 0.001$; Figure 1C and 1G).

Previously, mTORC1 and mTORC2 were also shown to regulate dendritic growth (Urbanska et al., 2012). Thus, we visualized dendrites in single-neuron cultures, where they can be well-resolved by immunostaining with an antibody against MAP2. We reconstructed the dendritic tree of each neuron and found that total dendritic length was reduced by both mTORC1 inactivation (Con: 1260 ± 116 µm, Rap-KO: 747 ± 70 µm, $p < 0.001$; Figure 1D), and mTORC2 inactivation (Con: 1035 ± 76 µm, Ric-KO: 815 ± 78 µm, $p = 0.043$; Figure 1H). These data verify that a reduction in mTORC1 or mTORC2 activity is sufficient to decrease neuronal soma area and dendritic length, which agrees with two previous studies comparing the effects of mTORC1 and mTORC2 inactivation (Angliker et al., 2015; Urbanska et al., 2012), and confirm that both mTOR complexes are required for proper neuronal morphology.

The decrease in soma size and dendritic length predicts that the passive membrane properties of Raptor-KO and Rictor-KO neurons will be altered. To test this, we performed current-clamp analysis of neurons from each group to assess alterations in passive membrane properties and action potential (AP) dynamics (Table 1). As may be expected from their decreased soma size, the input resistances of Raptor-KO and Rictor-KO neurons were increased compared with those of their respective controls (Con: 277 ± 37 MΩ, Rap-KO: 442 ± 33 MΩ, $p = 0.003$; Con: 237 ± 28 MΩ, Ric-KO: 329 ± 37 MΩ, $p = 0.033$). Also

reflective of their reduced soma size, the membrane capacitance (C_m) of Raptor-KO neurons was significantly lower than that of Raptor-Con neurons (Con: 138 ± 8.2 pF, Rap-KO: 87 ± 7.4 pF, $p < 0.001$); however, the effect of Rictor loss on reducing the C_m did not reach statistical significance (Con: 173 ± 14 pF, Ric-KO: 135 ± 10 pF, $p = 0.065$).

Table 1.

Raptor-KO				
	Con, n = 13	Rap-KO, n = 15	p value	95% CI of difference
Resting Potential, mV	53.3 ± 2.2	55.9 ± 2.0	0.38	-3.4 - 8.6
Input Resistance, MΩ	277 ± 37	442 ± 33	0.003	63 -268
Capacitance, pF	138 ± 8.2	87 ± 7.4	< 0.001	-73.2 - -27.8
Time constant, ms	36.8 ± 2.9	36.2 ± 2.6	0.89	-8.6 - 7.4
AP threshold, mV	37.1 ± 2.2	38.0 ± 2.0	0.76	-5.1 – 7.0
AP amplitude, mV	77.8 ± 3.5	67.7 ± 3.1	0.043	-19.7 - -0.34
Rictor-KO				
	Con, n = 15	Ric-KO, n = 17	p value	95% CI of difference
Resting Potential, mV	53.5 ± 1.1	52.2 ± 1.2	0.41	-4.5 - 1.8
Input Resistance, MΩ	237 ± 28	329 ± 37	0.033	6 - 176
Capacitance, pF	173 ± 14	135 ± 10	0.065	-78.6 - 2.7
Time constant, ms	37.4 ± 5.1	40.3 ± 5.2	0.65	-9.6 - 15.4
AP threshold, mV	35.0 ± 1.3	32.3 ± 1.3	0.14	-6.5 - 0.99
AP amplitude, mV	73.9 ± 3.2	69.0 ± 2.99	0.27	-13.8 – 4.1

Table 1. Summary of the measurements of basic membrane properties. Measurements are estimated marginal means ± s.e.m. Significance tested with Generalized Estimating Equations.

Deletion of *Raptor* decreases glutamatergic synaptic strength in single-neuron cultures by decreasing quantal size and synapse number.

To identify specific roles for mTORC1 and mTORC2 signaling in the regulation of glutamatergic synaptic transmission, we used a single-neuron culture system, which allows for the quantification of multiple parameters of pre- and postsynaptic function in the absence of network compensation and synaptic plasticity. We first performed whole-cell voltage-clamp recordings of glutamatergic neurons and evoked APs to examine evoked excitatory postsynaptic currents (eEPSCs) from Raptor-Con and Raptor-KO single neurons. Although the fast component tau of the eEPSC decay was unaltered (Con: 5.65 ± 0.32, Rap-KO: 5.67 ± 0.31, p = 0.45: Figure 2A_3), the eEPSC amplitudes were reduced by almost 60% in Raptor-KO neurons relative to those of Raptor-Con neurons (Con: 6.65 ± 1.38 nA, Rap-KO: 2.80 ± 0.57 nA, p = 0.003; Figure 2$A_{1,2}$), showing that intact mTORC1 signaling is necessary for normal evoked glutamatergic transmission.

The observed reduction in evoked synaptic strength following Raptor loss could be due to changes in the amplitude of the postsynaptic response to single SV fusion (quantal size) or the number of fusion-competent SVs (readily releasable pool, RRP). First, to test for changes in quantal size, we recorded the spontaneous release of miniature EPSCs (mEPSCs) and measured their amplitude and decay time constants, properties that are primarily dictated by postsynaptic ionotropic receptor levels and/or activity. Raptor-KO significantly decreased the mEPSC amplitude (Con: 27.8 ± 1.9 pA, Rap-KO: 21.5 ± 1.4 pA, p = 0.006; Figure 2$B_{1,2}$), but did not affect the decay time (Con: 3.48 ± 0.14 ms, Rap-KO: 3.40 ± 0.13 ms, p = 0.68; Figure 2B_3), when compared with those of Raptor-Con neurons. This reduction in quantal size implicates a postsynaptic impairment in Raptor-KO neurons that at least partially accounts for their decrease in evoked glutamatergic release.

Next, we assessed the number of SVs in the RRP following *Raptor* deletion, which can be directly quantified in a single neuron by applying a pulse of hypertonic sucrose (500 mM) to induce the

exocytosis of all of a neuron's fusion-competent vesicles (Rosenmund & Stevens, 1996). The integral of the transient current during sucrose application represents the total charge contained in the RRP, and the total number of vesicles in the RRP can then be calculated by dividing the total charge by the average charge of the miniature events from each neuron. We found that the sucrose-induced charge transfer, or the RRP charge, in glutamatergic Raptor-KO neurons was decreased by almost 60% compared with that of Raptor-Con neurons (Con: 767 ± 127 pC, Rap-KO: 337 ± 53 pC, p = 0.002; Figure $2C_{1,2}$). As a result, the mean number of SVs contained in the RRP of Raptor-KO glutamatergic neurons was reduced by almost 50% relative to that of Raptor-Con neurons (Con: 7145 ± 1415 vesicles, Rap-KO: 3664 ± 718 vesicles p = 0.008; Figure $2C_3$).

The observed decrease in the number of SVs in the RRP could be due to a decrease in the total number of synapses per neuron or to a decrease in the number of fusion-competent SVs per synapse. To distinguish between these possibilities, we visualized glutamatergic synapses and dendrites by immunostaining with antibodies against VGLUT1 and MAP2. We found that the number of glutamatergic synapses per neuron was decreased by approximately 40% due to Raptor loss (Con: 721 ± 106 synapses/neuron, Rap-KO: 430 ± 65 synapses/neuron, p = 0.02; Figure $2D_{1,2}$). However, based on the mean values for the RRP and number of synapses, we estimated similar numbers of fusion-competent SVs per synapse in Raptor-Con neurons (9.91 SVs/synapse) and Raptor-KO neurons (8.52 SVs/synapse). Taken together, these data suggest that the reduction in the RRP caused by *Raptor* loss is due to an impairment in synapse formation or maintenance, and not the number of SVs at each synapse.

Figure 2

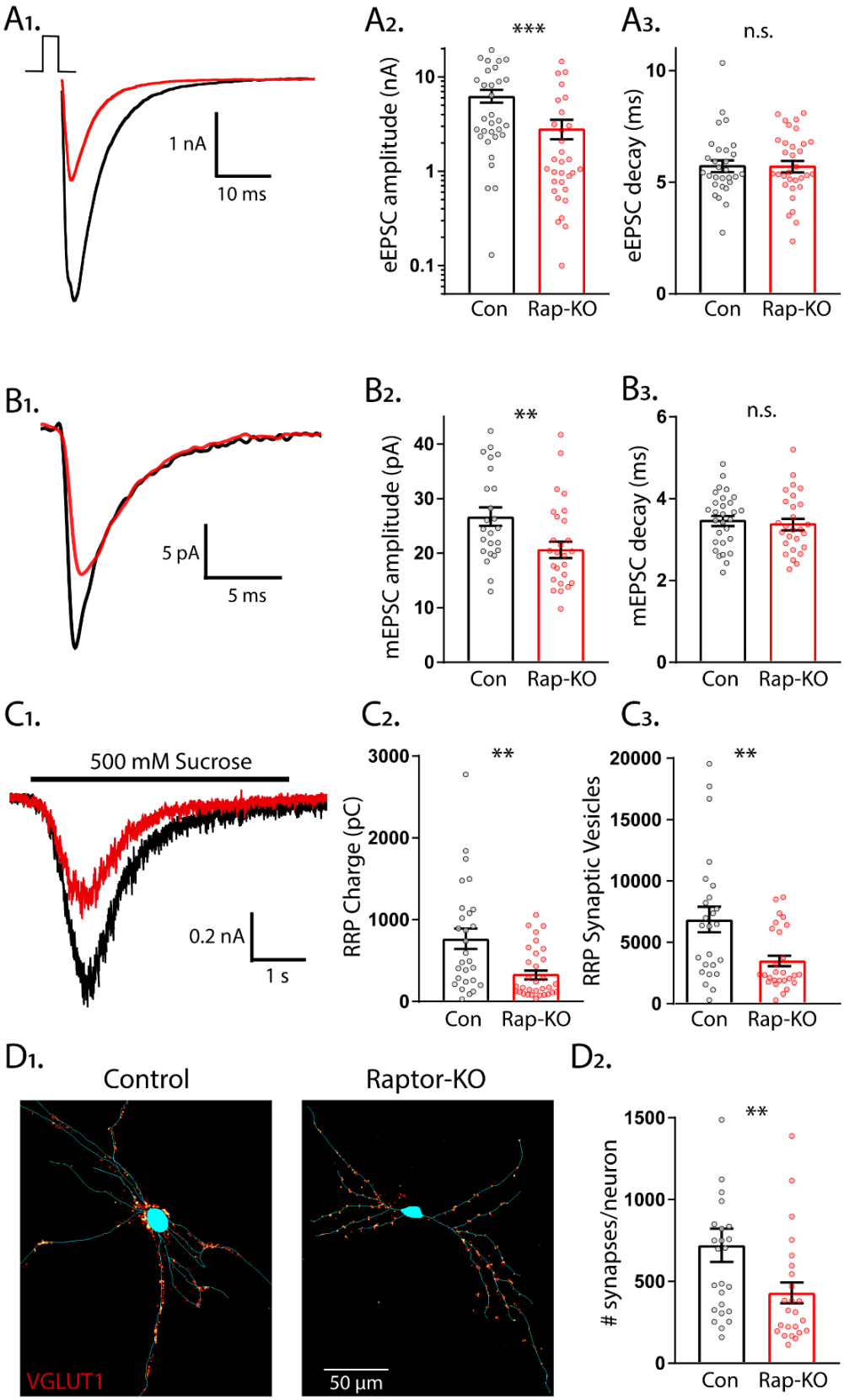

232

Figure 2. Loss of Raptor decreases the strength of evoked excitatory synaptic transmission via changes in quantal size and synapse number. A_1. Example traces of evoked EPSCs recorded from single-neuron primary hippocampal cultures of Raptor-Con (black) and Raptor-KO (red) neurons. A_2. Plot showing the values of peak EPSC amplitudes recorded from Raptor-Con (black) and Raptor-KO (red) neurons on a logarithmic scale. A_3. Plot showing the values of single exponential fits to the fast component of the EPSC decay recorded from Raptor-Con (black) and Raptor-KO (red) neurons on a linear scale. B_1. Example traces of average miniature EPSCs recorded from single-neuron primary hippocampal cultures of Raptor-Con (black) and Raptor-KO (red) neurons. B_2. Plot showing the values of mEPSC peak amplitudes recorded from Raptor-Con (black) and Raptor-KO (red) neurons. B_3. Plot showing the distributions of mEPSC decay time constants recorded from Raptor-Con (black) and Raptor-KO (red) neurons. C_1. Example traces of the current response to 500 mM sucrose application recorded from single-neuron primary hippocampal cultures of Raptor-Con (black) and Raptor-KO (red) neurons. The black line indicates the time of sucrose application. C_2. Plot showing the values of the charge contained in the readily releasable pool (RRP) of Raptor-Con (black) and Raptor-KO (red) neurons, as determined by integrating the sucrose response after subtracting the steady state component. C_3. Plot showing the number of vesicles contained in the RRP of Raptor-Con (black) and Raptor-KO (red) neurons, as determined by dividing the RRP charge by the mean mEPSC charge for each neuron. D_1. Representative images showing fluorescence intensity in a red color look up table (LUT) from VGLUT1 immunostaining superimposed on a tracing of the cell body and dendrites from a Raptor-Con (left) and a Raptor-KO (right) neuron. D_2. Plot showing the values of synapse number per neuron for Raptor-Con (black) and Raptor-KO (red) neurons. For all dot plots, each dot represents the mean response from one neuron and the bars show the estimated marginal means and standard errors. ** indicates a p value of <0.01, *** indicates $p < 0.001$ and n.s. indicates $p > 0.05$, as tested with Generalized Estimating Equations.

Deletion of *Rictor* decreases glutamatergic synaptic strength in single-neuron cultures without affecting quantal size and synapse number.

Next, we examined eEPSCs from Rictor-Con and Rictor-KO single neurons. Like Raptor-KO neurons, the eEPSC amplitudes were reduced by almost 60% relative to Rictor-Con neurons (Con: 4.70 ± 0.78 nA, Ric-KO: 1.90 ± 0.57 nA, p = 0.001; Figure $3A_{1,2}$), with no effect on the fast component decay time (Con: 5.25 ± 0.25, Ric-KO: 5.53 ± 0.24, p = 0.55: Figure $3A_3$). Because of this similarity in the effect on the evoked response, and because our immunostaining indicated that loss of *Rictor* decreased mTORC1 activity, we hypothesized that the physiological mechanisms would be shared (i.e. quantal size and synapse number reductions). Instead, we found that mTORC2 inhibition via *Rictor* loss did not significantly affect the mEPSC amplitude (Con: 19.9 ± 1.1 pA, Ric-KO: 17.7 ± 0.9 pA, p = 0.11; Figure $3B_{1,2}$) or decay time (Con: 3.14 ± 0.11 ms, Ric-KO: 3.10 ± 0.10 ms, p = 0.76; Figure $3B_3$) relative to those of Rictor-Con neurons, suggesting that, unlike in Raptor-KO neurons, quantal size alterations do not contribute to the decreased glutamatergic synaptic strength observed following loss of *Rictor*.

We next determined whether alterations in the RRP size contributed to the reduced eEPSC amplitude in Rictor-KO neurons. The sucrose-induced charge transfer and the number of SVs in the RRP were decreased following *Rictor* deletion, although only by approximately 35% (Con: 474 ± 59 pC, Ric-KO: 304 ± 37 pC, p = 0.011; and Con: 6441 ± 857 vesicles, Ric-KO: 4178 ± 535 vesicles, p = 0.024; Figure $3C_{1-3}$). In contrast to the reduced synapse number caused by *Raptor* loss, the number of glutamatergic synapses per neuron was not decreased by *Rictor* loss (Con: 764 ± 133 synapses/neuron, Ric-KO: 771 ± 140 synapses/neuron, p = 0.97; Figure $3D_{1,2}$), even though total dendritic length was reduced (Figure 1H). Based on these numbers, we estimated that the number of fusion-competent SVs per synapse was reduced from 8.43 SVs/synapse in Rictor-Con neurons to 5.42 SVs/synapse in Rictor-KO neurons, which would partially account for the 60% reduction in eEPSC amplitude. Thus, although mTORC1 and mTORC2

281 inactivation both decreased eEPSC strength, our data suggest that the underlying physiological

282 mechanisms are quite different.

Figure 3

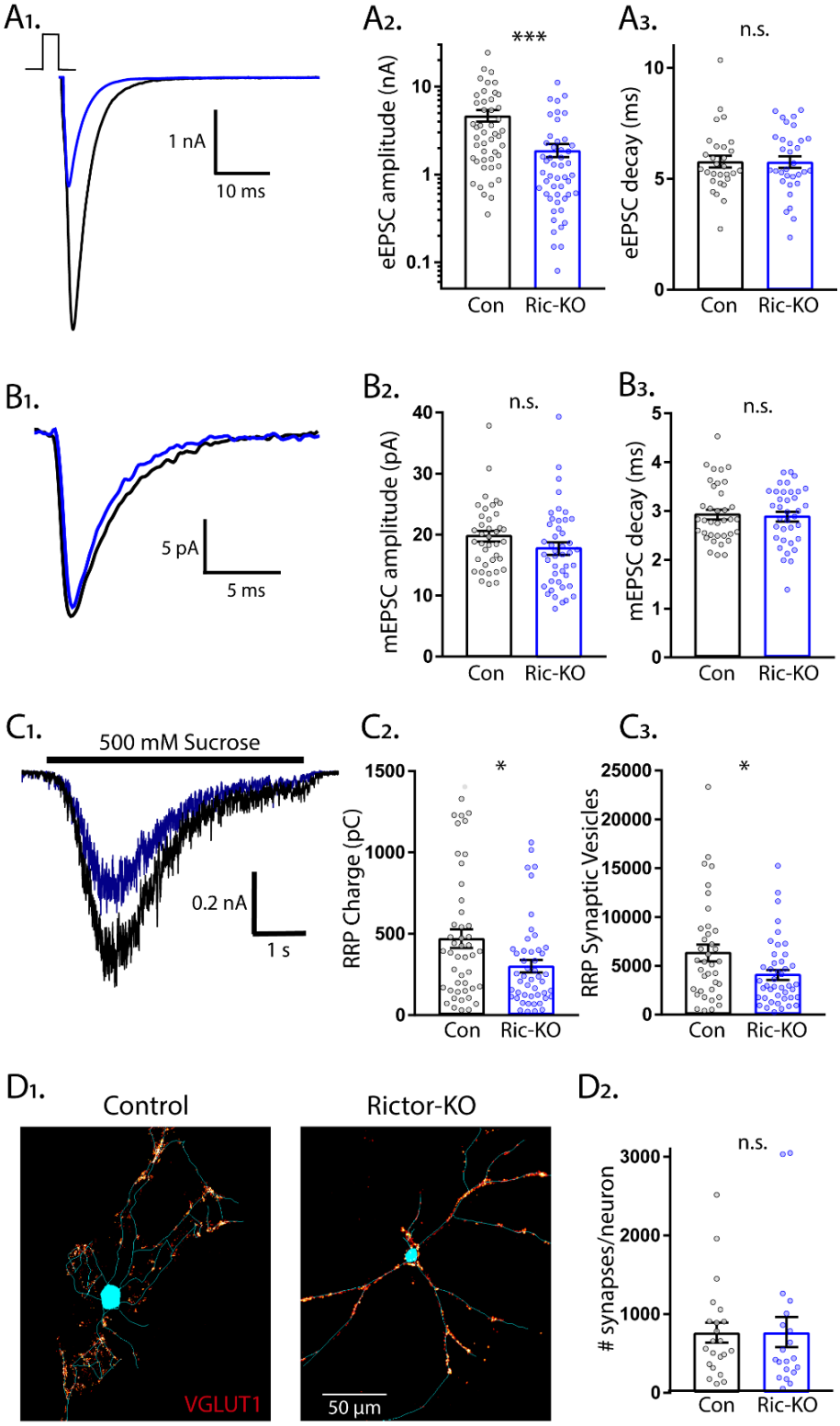

Figure 3. Loss of Rictor decreases the strength of evoked excitatory synaptic transmission without altering quantal size or synapse number. A_1. Example traces of evoked EPSCs recorded from single-neuron primary hippocampal cultures of Rictor-Con (black) and Rictor-KO (blue) neurons. A_2. Plot showing the values of peak EPSC amplitudes recorded from Rictor-Con (black) and Rictor-KO (blue) neurons on a logarithmic scale. A_3. Plot showing the values of single exponential fits to the fast component of the EPSC decay recorded from Rictor-Con (black) and Rictor-KO (blue) neurons on a linear scale. B_1. Example traces of average miniature EPSCs recorded from single-neuron primary hippocampal cultures of Rictor-Con (black) and Rictor-KO (blue) neurons. B_2. Plot showing the values of mEPSC peak amplitudes recorded from Rictor-Con (black) and Rictor-KO (blue) neurons. B_3. Plot showing the distributions of mEPSC decay time constants recorded from Rictor-Con (black) and Rictor-KO (blue) neurons. C_1. Example traces of the current response to 500 mM sucrose application recorded from single-neuron primary hippocampal cultures of Rictor-Con (black) and Rictor-KO (blue) neurons. The black line indicates the time of sucrose application. C_2. Plot showing the values of the charge contained in the readily releasable pool (RRP) of Rictor-Con (black) and Rictor-KO (blue) neurons, as determined by integrating the sucrose response after subtracting the steady state component. C_3. Plot showing the number of vesicles contained in the RRP of Rictor-Con (black) and Rictor-KO (blue) neurons, as determined by dividing the RRP charge by the mean mEPSC charge for each neuron. D_1. Representative images showing fluorescence intensity in a red color look up table (LUT) from VGLUT1 immunostaining superimposed on a tracing of the cell body and dendrites from a Rictor-Con (left) and a Rictor-KO (right) neuron. D_2. Plot showing the values of synapse number per neuron neuron for Rictor-Con (black) and Rictor-KO (blue) neurons. For all dot plots, each dot represents the mean response from one neuron and the bars show the estimated marginal means and standard errors of the mean. ** indicates a p value of <0.01, *** indicates p < 0.001 and n.s. indicates p > 0.05, as tested with Generalized Estimating Equations.

Rictor loss decreases the probability and rate of evoked SV release and increases paired pulse ratios, but Raptor loss does not.

For Raptor-KO neurons, the combined decreases in quantal size and the number of SVs in the RRP may be sufficient to account for the magnitude of the decrease in the evoked glutamatergic

response. For Rictor-KO neurons, however, the decrease in the evoked glutamatergic response was greater than the decrease in the RRP, indicating that evoked SV release itself may also be impaired. We tested this in three ways. First, we calculated the probability that an SV fuses in response to an AP (vesicular release probability, P_{vr}) by dividing the number of vesicles released in response to AP stimulation by the number of vesicles in the RRP. The P_{vr} was not different between Raptor-KO and Raptor-Con neurons (Con: 0.092 ± 0.012, Rap-KO: 0.086 ± 0.012, p = 0.72; Figure 4A). However, Rictor-KO neurons showed a reduced P_{vr} from 0.118 ± 0.013, in Rictor-Con neurons, to 0.083 ± 0.009 (p = 0.010; Figure 4D), suggesting that Rictor loss reduces the probability of evoked vesicle fusion. Next, we calculated the peak rate at which SVs were released during the eEPSC by deconvolving the eEPSC with the mean mEPSC shape for each neuron (Aumann & Parnas, 1991; Diamond & Jahr, 1995; Schneggenburger & Neher, 2000). Again, we found no effect of mTORC1 inactivation (Con: 26.0 ± 3.3 s^{-1}, Rap-KO: 26.1 ± 3.2 s^{-1}, p = 0.98; Figure $4B_{1,2}$), but mTORC2 inactivation decreased the maximum rate of SV release from 22.8 ± 3.38 s^{-1} in Rictor-Con neurons, to 11.0 ± 1.6 s^{-1} in Rictor-KO neurons (p = 0.001; Figure $4E_{1,2}$).

As a third test of SV release changes, we evoked two presynaptic APs in close succession and divided the second postsynaptic response by the first to measure paired-pulse ratios (PPRs) at 25, 50, 100, and 200 ms interstimulus intervals (ISIs) for each neuron group. Generally, in neurons with a lower P_{vr}, the second stimulus evokes a larger response than that evoked by the first, resulting in a higher PPR. Conversely, in neurons with a higher P_{vr}, the second stimulus evokes a smaller response than that evoked by the first, resulting in a lower P_{vr}. In agreement with the P_{vr} measurements, there was no effect of Raptor loss on PPRs at any of the ISIs tested (main effect of group, p = 0.35; Figure $4C_{1,2}$). Similarly consistent with the P_{vr} measurements, the Rictor-KO neurons, which had a reduced P_{vr}, showed a significant increase in PPRs at all ISIs tested compared with those of Rictor-Con neurons (main effect of group, p < 0.001; Figure $4F_{1,2}$). Taken together, these data indicate that the reductions in quantal size

333 and SV number in the RRP of Raptor-KO neurons account for the decreased eEPSC amplitude following

334 inactivation of mTORC1. More importantly, our results strongly suggest that Rictor, but not Raptor, loss

335 leads to presynaptic impairments in evoked vesicle release.

Figure 4

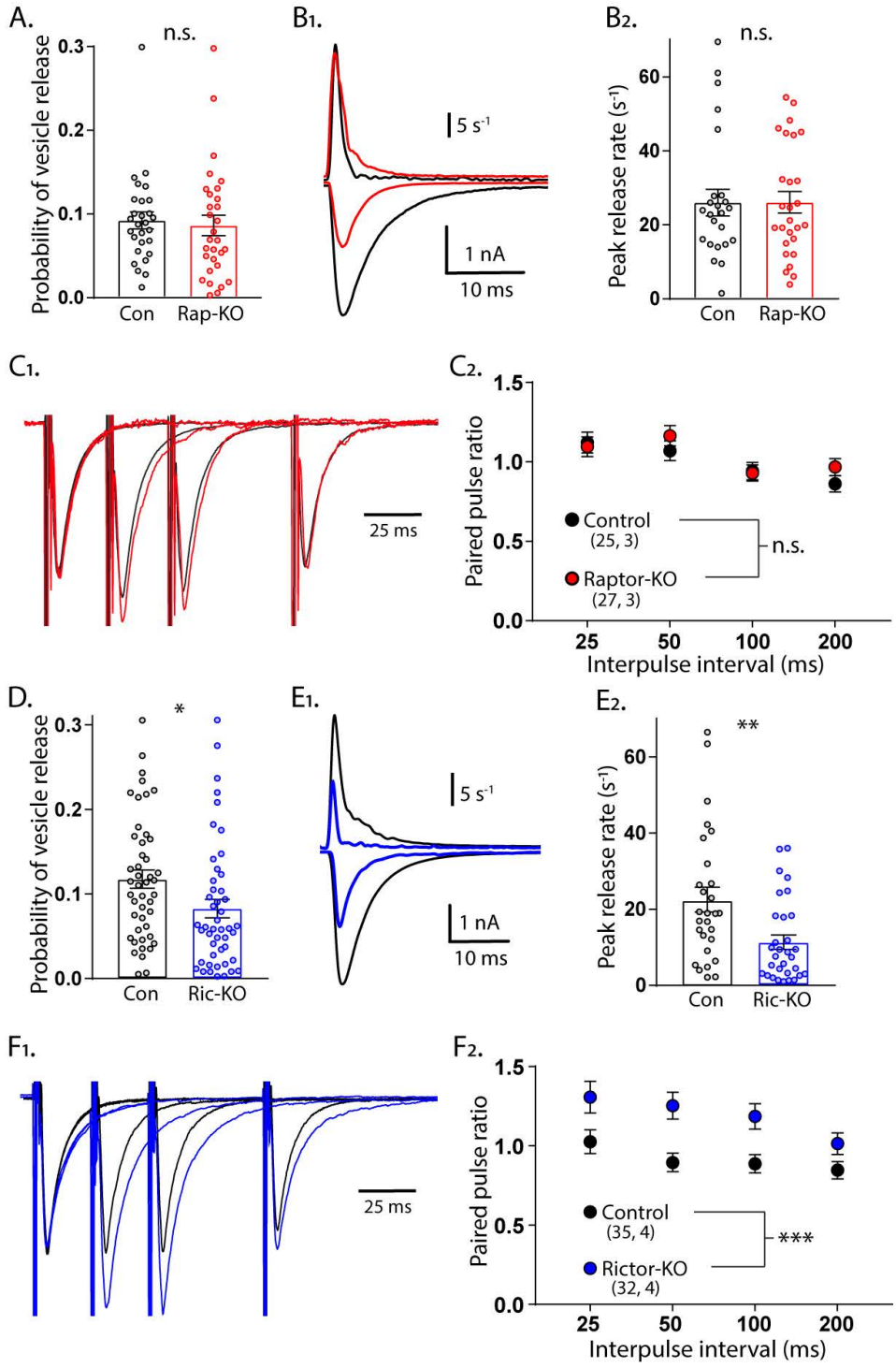

Figure 4. Loss of Rictor reduces evoked SV release efficiency but Raptor loss does not. A. Plot showing no difference in the vesicular release probability of Raptor-Con (black) and Raptor-KO (red) neurons. B_1. Example traces showing the rate of SV release (top traces) over their corresponding EPSCs from Raptor-Con (black) and Raptor-KO (red) neurons. B_2. Plot of the peak vesicle release rates of Raptor-Con (black) and Raptor-KO (red) neurons. C_1. Example traces of EPSCs evoked in response to 2 ms depolarizations spaced at 25, 50, and 100 ms. The three sweeps at different intervals are overlayed, as are the responses from Raptor-Con (black) and Raptor-KO (red) neurons. The values are normalized to the peak amplitude of the first EPSC in each sweep. C_2. Summary data showing the estimated marginal means and standard errors for Raptor-Con (black) and Raptor-KO (red) groups at different interpulse intervals. D. Plot showing the decrease in vesicular release probability between Rictor-Con (black) and Rictor-KO (blue) neurons. E_1. Example traces showing the rate of SV release (top traces) over their corresponding EPSCs from Rictor-Con (black) and Rictor-KO (blue) neurons. E_2. Plot of the peak vesicle release rates of Raptor-Con (black) and Raptor-KO (red) neurons. F_1. Example traces of EPSCs evoked in response to 2 ms depolarizations spaced at 25, 50, and 100 ms. The three sweeps at different intervals are overlayed, as are the responses from Rictor-Con (black) and Rictor-KO (blue) neurons. The values are normalized to the peak amplitude of the first EPSC in each sweep. F_2. Summary data showing the estimated marginal means and standard errors for Rictor-Con (black) and Raptor-KO (red) groups at different interpulse intervals. * indicates $p < 0.05$, ** indicates $p < 0.01$, *** indicates $p < 0.001$, and n.s. = $p > 0.05$, effect of group tested with Generalized Estimating Equations.

Postsynaptic loss of Raptor recapitulates the decrease in evoked EPSC amplitude, but Rictor does not.

The experiments in the single-neuron cultures indicate that the effects of Raptor loss on eEPSCs are mainly postsynaptic, whereas those of Rictor loss are mainly presynaptic. In single-neuron cultures, however, the pre- and postsynaptic compartments are genetically identical, making it difficult to definitively determine whether a synaptic change is pre- or postsynaptic. To test the hypothesis that mTORC1 regulates eEPSC strength via postsynaptic mechanisms, whereas mTORC2 does not, we recorded postsynaptic responses simultaneously in pairs of control and Raptor-KO or Rictor-KO neurons evoked by optogenetic stimulation of wild-type neurons in a traditional mass-neuron culture (Figure 5A). We found that the light-evoked (le)EPSC amplitudes evoked onto Raptor-KO neurons were significantly smaller than those onto partner control neurons (Con: 330 ± 63 pA, Rap-KO: 146 ± 28 pA, $p < 0.001$; Figure $5B_{1\text{-}3}$). Moreover, the magnitude of this decreased amplitude was equivalent to that initially observed in the eEPSCs recorded from the Raptor-KO single-neuron culture, at almost 60%. Conversely, the leEPSC amplitudes evoked onto Rictor-KO neurons were unaltered relative to those of control neurons (Con: 353 ± 92 pA, Ric-KO: 357 ± 93 pA, $p = 0.97$; Figure $5C_{1\text{-}3}$). These data suggest that Raptor, but not Rictor, is required at the postsynapse to facilitate evoked glutamatergic synaptic transmission.

Figure 5

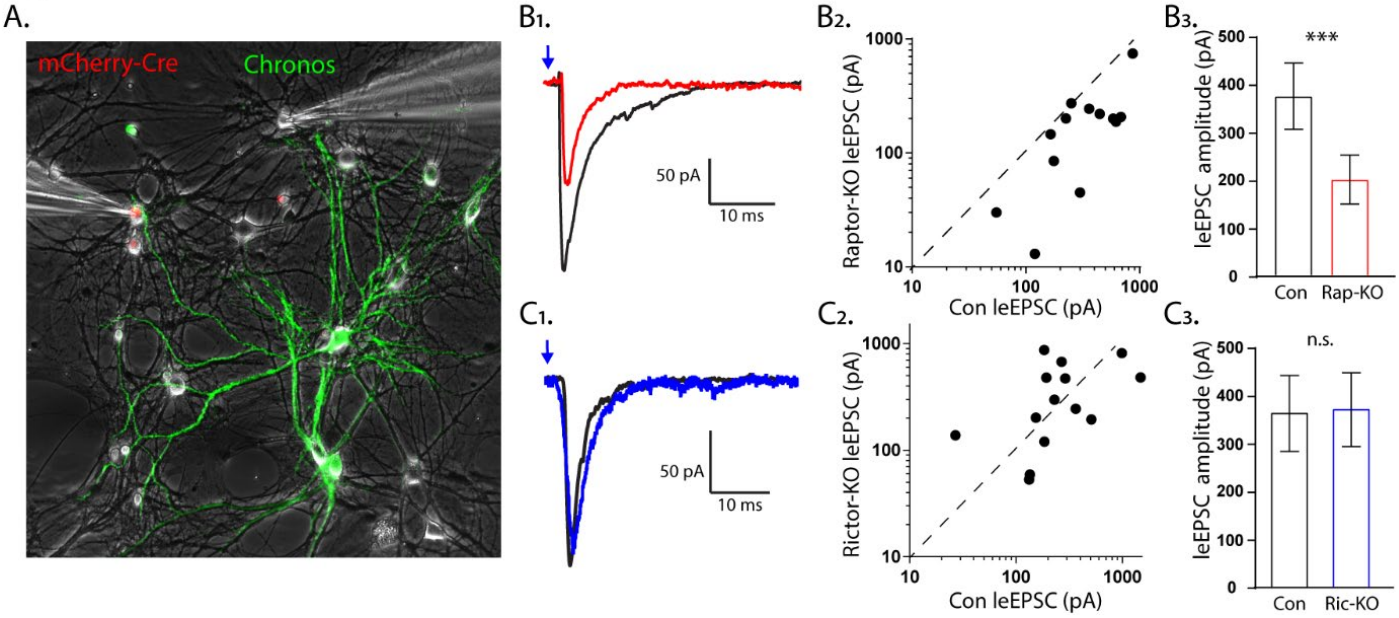

Figure 5. The effect of Raptor loss on evoked EPSCs, but not Rictor, is due to postynaptic impairments.

A_1. Representative image illustrating the experimental setup. The red fluorescence from the mCherry-Cre and the green fluorescence from the optogenetic protein Chronos fused to GFP are shown overlayed on a phase contrast image showing the patch pipettes attached to one Cre-positive (left pipette) and one Cre-negative (right pipette) neuron. B_1. Example light-evoked (le)EPSCs obtained simultaneously from a control (black) and a Raptor-KO (red) neuron held at -55 mV in response to a 2 ms flash of blue light. B_2. Scatter plot showing the leEPSC responses of neuron pairs to blue light stimulation. The peak amplitude from the control neuron in each pair is represented by the symbol's value on the x-axis, and the peak amplitude of the Raptor-KO neuron is represented by the symbol's value on the y-axis. Pairs in which the KO response is smaller than the control response will be below the dashed line. B_3. Bar graph showing the leEPSC amplitudes (mean ± s.e.m.) of control (black) and Raptor-KO (red) neurons. C_1. Example leEPSCs obtained simultaneously from a control (black) and a Rictor-KO (blue) neuron held at -55 mV in response to a 2 ms flash of blue light. C_2. Scatter plot showing the leEPSC responses of neuron pairs to blue light stimulation. The peak amplitude from the control neuron in each pair is represented by the symbol's value on the x-axis, and the peak amplitude of the Rictor-KO neuron is represented by the symbol's value on the y-axis. C_3. Bar graph showing the leEPSC amplitudes (mean ± s.e.m.) of control (black) and Rictor-KO (blue) neurons. *** indicates $p < 0.001$ and n.s. = $p > 0.05$, effect of group tested with Generalized Estimating Equations.

mTORC1 regulates the rate constant for spontaneous SV fusion, but mTORC2 does not.

Thus far, we have shown that inactivation of mTORC1 or mTORC2 reduced both evoked EPSC amplitude and RRP size, however, impairments to evoked SV fusion were only observed following mTORC2 inactivation. A decrease in the number of vesicles in the RRP often leads to a decrease in both evoked and spontaneous release, because there is a decreased number of SVs available for fusion, either in response to an action potential or spontaneously (Schneggenburger & Rosenmund, 2015). To assess whether spontaneous release is altered by mTORC1 or mTORC2 inactivation, we recorded the frequency of mEPSC events in single-neuron cultures, and then calculated the spontaneous release rate constant (SRR) by dividing the miniature event frequency by the number of SVs in the RRP for each neuron. The SRR is the rate at which an individual SV fuses with the plasma membrane in the absence of stimulation, and the reciprocal of the rate constant is the mean dwell time of an SV in the RRP before it fuses spontaneously. Despite the strong reduction in the RRP caused by loss of synapses in Raptor-KO neurons, the mEPSC frequency was not decreased (Con: 5.77 ± 0.82 Hz, Rap-KO: 6.15 ± 0.87 Hz, p = 0.82; Figure 6$A_{1,2}$). However, the SRR was significantly increased in Raptor-KO neurons (Con: 0.942 ± 0.18E-3 s^{-1}, Rap-KO: 1.751 ± 0.31E-3 s^{-1}, p = 0.01; Figure 6A_3), corresponding to mean dwell times of 1062 s and 571 s per SV in Raptor-Con and Raptor-KO neurons, respectively. In Rictor-KO neurons, the mEPSC frequency was decreased relative to Rictor-Con neurons (Con: 3.61 ± 0.89 Hz, Ric-KO: 2.11 ± 0.50 Hz, p = 0.012; Figure 6$B_{1,2}$), but, because of the decrease in the RRP, the SRR was unchanged (Con: 1.14 ± 0.21E-3 s^{-1}, Ric-KO: 0.79 ± 0.13E-3 s^{-1}, p = 0.15; Figure 6B_3).

Next, we wanted to assess the effect of mTOR inactivation on spontaneous release rates under conditions in which the SRR is elevated. To do this, we stimulated neurons at 10 Hz and then measured spontaneous release in the 10 seconds following the AP train. Compared to baseline spontaneous release, 10 Hz stimulation caused an increase in spontaneous SV fusion in the 10 seconds following the end of the train in all groups tested (compare Figure 6A_3 and B_3 to Figure 6C_2 and 6D_2). Importantly, the

mean SRR of Raptor-KO neurons after 10 Hz trains was still higher than that of Raptor-Con neurons (Con: 2.24 ± 0.086E-3 s^{-1}, Rap-KO: 5.09 ± 1.07E-3 s^{-1}, p = 0.001; Figure 6$C_{1,2}$), whereas the SRR following 10 Hz trains in Rictor-KO neurons was not significantly different from that of Rictor-Con neurons (Con: 2.64 ± 0.56E-3 s^{-1}, Ric-KO: 1.61 ± 0.33E-3 s^{-1}, p = 0.096; Figure 6$D_{1,2}$). Taken together, these data indicate that, although mTORC1 inactivation reduces the RRP size, the mEPSC frequency is maintained due to an increased rate of spontaneous SV release.

Figure 6

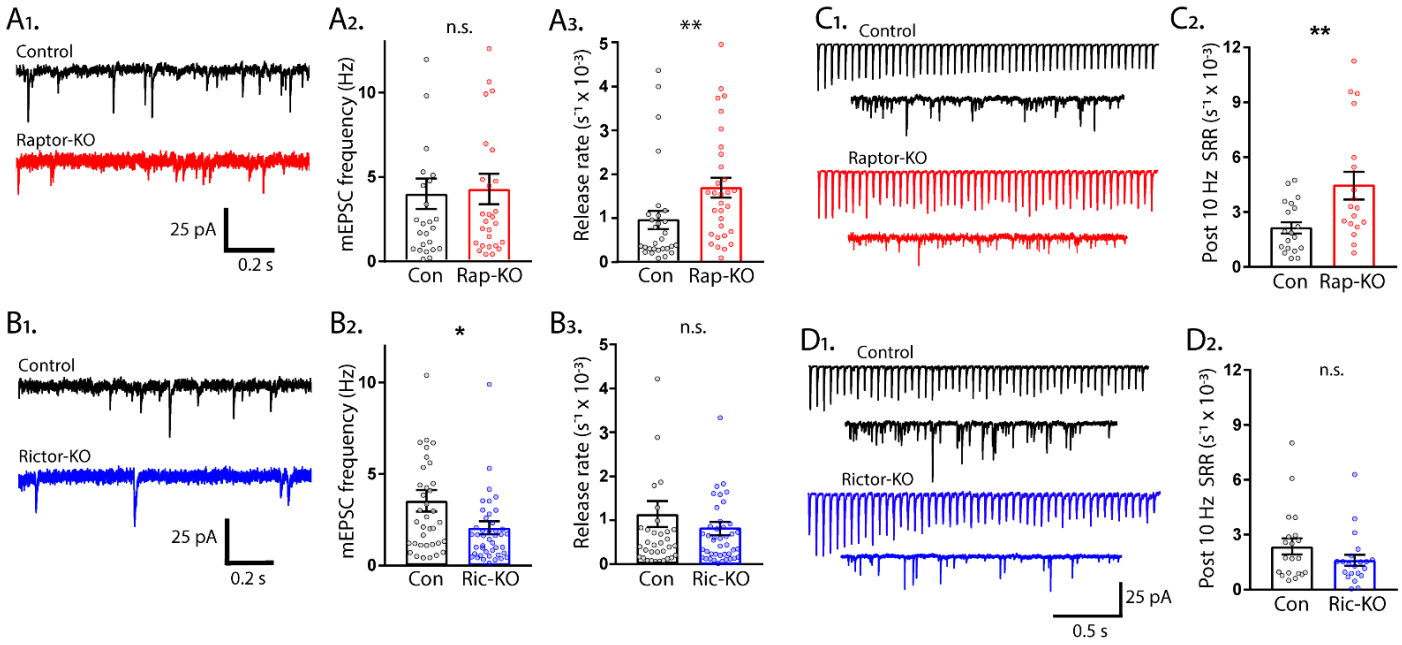

Figure 6. The rate constant for spontaneous vesicle fusion is regulated by mTORC1 activity. A_1. Example traces of miniature synaptic currents recorded in single-neuron cultures of Raptor-Con (black) and Raptor-KO (red) neurons. A_2. Plot showing the mEPSC frequencies from Raptor-Con (black) and Raptor-KO (red) neurons. A_3. Plot showing the spontaneous release rate (SRR) of Raptor-Con (black) and Raptor-KO (red) neurons. B_1. Example traces of miniature synaptic currents recorded in single-neuron cultures of Rictor-Con (black) and Rictor-KO (blue) neurons. B_2. Plot showing the mEPSC frequencies from Rictor-Con (black) and Rictor-KO (blue) neurons. B_3. Plot showing the spontaneous release rate (SRR) of Rictor-Con (black) and Rictor-KO (blue) neurons. C_1. Example traces of EPSCs in response to 50 stimulations at 10 Hz (top traces) over traces of spontaneous SV release in the 10 s

following the train. Example trace from a Raptor-Con neuron is in black, and a Raptor-KO neuron in red. C_2. Plot showing the rate constants for spontaneous SV release of Raptor-Con (black) and Raptor-KO (red) neurons in the 10 s following the 10 Hz stimulation. D_1. Example traces of EPSCs in response to 50 stimulations at 10 Hz (top traces) over traces of spontaneous SV release in the 10 s following the train. Example trace from a Rictor-Con neuron is in black, and a Rictor-KO neuron in blue. D_2. Plot showing the rate constants for spontaneous SV release of Rictor-Con (black) and Rictor-KO (blue) neurons in the 10 s following the 10 Hz stimulation. In the dot plots, each dot represents the value from one neuron, and the bars show the estimated marginal means and s.e.m. * = $p < 0.05$, ** = $p < 0.01$, and n.s. = $p > 0.05$, as tested with Generalized Estimating Equations.

Finally, we wanted to ensure that the regulation of SRR by mTORC1 was not unique to the single-neuron culture preparation, but quantification of the SRR in this manner is not possible in mass cultures or brain slice preparations. Instead, we measured mEPSC frequencies after treatment of the neurons with the mTOR inhibitor rapamycin at a time point (12 h) and concentration (20 nM) at which there should be no change in the number of vesicles in the RRP (Weston, Chen, & Swann, 2012). Under these assumptions, changes in mEPSC frequency should reflect changes in the SRR due to mTORC1 activity. After 12 h rapamycin treatment, the mEPSC frequency increased from 4.19 ± 0.60 Hz, in control, to 6.56 ± 0.94 Hz ($p = 0.016$, data not shown), a shift similar in magnitude to the one caused by *Raptor* deletion, indicating that mTORC1 inhibition increases the rate of spontaneous SV release, regardless of neuron culture conditions.

Figure S1

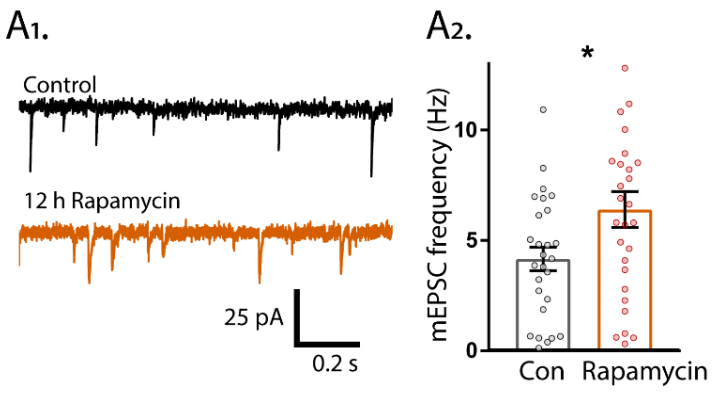

Figure S1. 12 h Rapamycin treatment increases mEPSCs. A_1. Example traces of mEPSC activity recorded in mass cultures after 12 h treatment with DMSO (black trace) or 20 nM rapamycin (orange trace). A_2. Summary data showing the increase in mEPSC frequency.

mTORC1 and mTORC2 oppositely regulate asynchronous SV fusion.

The rates of SV fusion vary over a range of several orders of magnitude, from approximately 0.001 s^{-1} at resting $[Ca^{2+}]_i$ for spontaneous release to approximately 20 s^{-1} during AP-evoked transmitter release at several micromolar of $[Ca^{2+}]_i$ (Sakaba & Neher, 2001; Schneggenburger & Neher, 2000; Sudhof, 2012). The data thus far indicate that mTORC1 and mTORC2 regulate the lowest (spontaneous) and highest (AP-evoked) SV fusion rates, respectively. Thus, we next tested how mTORC1 and mTORC2 inactivation affect SV release under conditions in which rate constants are expected to be between these two extremes, asynchronous SV release after a single stimulus and asynchronous fusion during repetitive stimulation, and upon sucrose-evoked fusion, which is calcium-independent.

Asynchronous SV release after a single stimulus in hippocampal neurons accounts for a low percentage of the total transmitter release, but may play important roles in neurotransmission (Kaeser & Regehr, 2014). To quantify the rate constant of asynchronous release, we subtracted the fast component of evoked release from the total EPSC charge and normalized it by the total RRP charge. Like the SRR, Raptor-KO neurons also showed an increase in the rate of asynchronous SV fusion relative to that of Raptor-Con neurons (Con: 0.070 ± 0.011 s^{-1}, Rap-KO: 0.122 ± 0.018 s^{-1}, p = 0.002; Figure $7A_{1,2}$). In contrast to Raptor-KO neurons, but similar to the effect of *Rictor* loss on the peak evoked SV fusion rate, Rictor-KO neurons showed a decrease in the asynchronous SV fusion rate relative to that of Rictor-Con neurons (Con: 0.096 ± 0.017 s^{-1}, Ric-KO: 0.047 ± 0.009 s^{-1}, p = 0.018; Figure $7B_{1,2}$).

Asynchronous release during high frequency stimulation can reach high rates of SV fusion, second only to synchronous evoked release. To quantify the asynchronous release rate during 10 Hz stimulation, we subtracted the fast component of evoked release from the total evoked EPSC of the last stimulation of 50 at 10 Hz and normalized this rate by the estimated remaining RRP charge. In this mode of SV release, Raptor-KO neurons did not show an elevated rate of fusion (Con: 1.15 ± 0.32 s^{-1}, Rap-KO: 1.23± 0.32 s^{-1}, p = 0.87; Figure $7C_{1,2}$), but Rictor-KO neurons did show a significantly lower rate of fusion

496 (Con: 2.21 ± 0.48 s^{-1}, Ric-KO: 1.19 ± 0.24 s^{-1}, p = 0.037; Figure 7$D_{1,2}$), relative to those of their respective

497 controls.

Figure 7

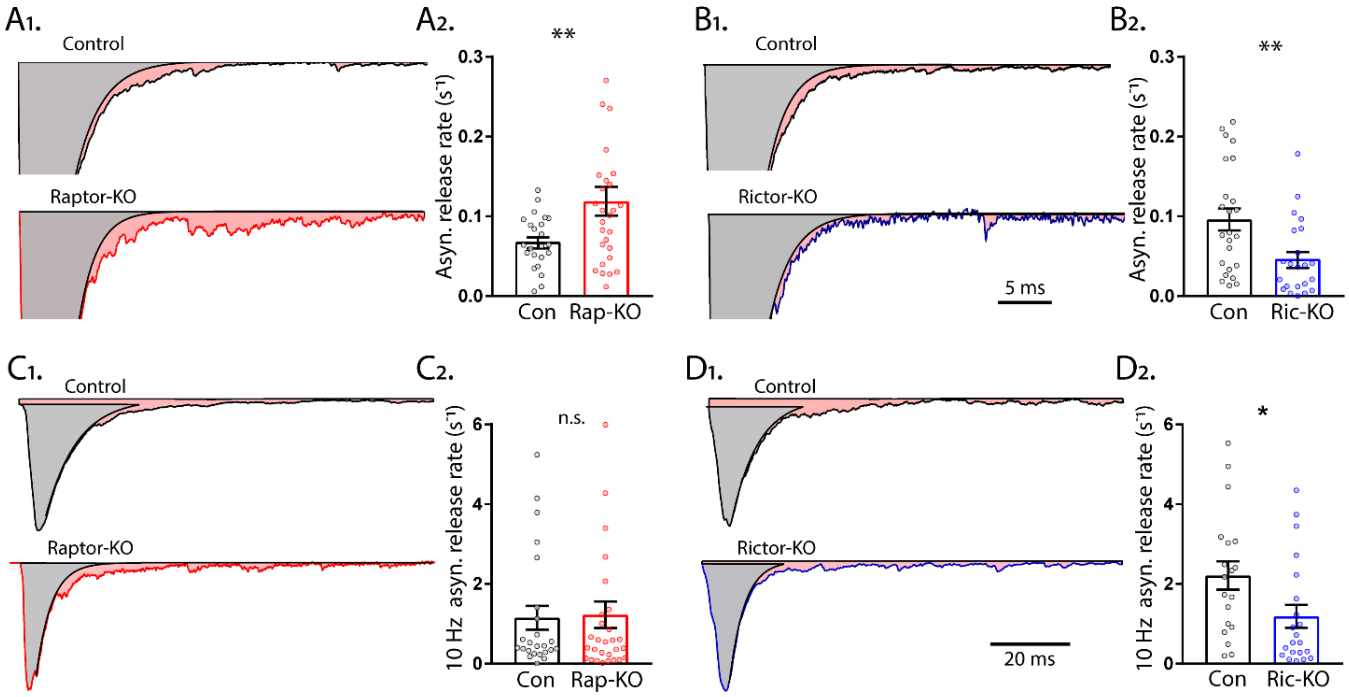

498 **Figure 7. mTORC1 and mTORC2 inactivation have opposite effects on asynchronous synaptic vesicle**

499 **release.** A_1. Example traces of normalized EPSCs evoked at 0.1 Hz from Raptor-Con (black) and Raptor-KO (red)

500 neurons. The gray shaded area represents the area under the curve of the synchronous component of synaptic

501 vesicle (SV) release, and the pink shaded area represents the asynchronous component. A_2. Plot showing the rate

502 constants for asynchronous SV release of Raptor-Con (black) and Raptor-KO (red) neurons. B_1. Example traces of

503 normalized EPSCs evoked at 0.1 Hz from Rictor-Con (black) and Rictor-KO (blue) neurons shaded to highlight the

504 synchronous (gray) and asynchronous (pink) components of SV release. B_2. Plot showing the rate constants for

505 asynchronous SV release of Rictor-Con (black) and Rictor-KO (blue) neurons. C_1. Example traces of normalized

506 EPSCs at the end of a 10 Hz train from Raptor-Con (black) and Raptor-KO (red) neurons. The gray shaded area

507 represents the area under the curve of the synchronous component of SV release and the pink shaded area

508 represents the asynchronous component. C_2. Plot showing the rate constants for asynchronous SV release at the

509 end of a 10 Hz train from Raptor-Con (black) and Raptor-KO (red) neurons. D_1. Example traces of normalized EPSCs

at the end of a 10 Hz train from Rictor-Con (black) and Rictor-KO (blue) neurons shaded to highlight the synchronous (gray) and asynchronous (pink) components of SV release. D_2. Plot showing the rate constants for asynchronous SV release at the end of a 10 Hz train from Rictor-Con (black) and Rictor-KO (blue) neurons. In the dot plots, each dot represents the mean value from one neuron, and the bars show the estimated marginal means and s.e.m. * = $p < 0.05$, ** = $p < 0.01$, and n.s. = $p > 0.05$, as tested with Generalized Estimating Equations.

To determine whether mTORC inactivation affects release rates in a mode of SV release that is calcium-independent, we analyzed the kinetics of the sucrose response to quantify the peak rate of SV release in response to 500 mM sucrose application, which is thought to reflect the calcium-independent energy barrier for SV fusion (Basu, Betz, Brose, & Rosenmund, 2007). This was done by integrating the responses to sucrose for each neuron, converting it to vesicle number and normalizing it to its corresponding RRP, and then finding the maximal slope as a measure for peak release rate (Basu et al., 2007). We found that the peak release rate constant induced by sucrose was not different between Raptor-Con and Raptor-KO neurons (Con: 1.54 ± 0.07 s^{-1}, Rap-KO: 1.50 ± 0.06 s^{-1}, $p = 0.76$; Figure $8A_{1,2}$), or Rictor-Con and Rictor-KO neurons (Con: 1.48 ± 0.15 s^{-1}, Ric-KO: 1.5 ± 0.17 s^{-1}, $p = 0.76$; Figure $8B_{1,2}$), indicating that the alteration in SV release caused by mTORC1 and mTORC2 inactivation are not due to alterations in the energy barrier for SV fusion, but instead they are due to alterations in the calcium sensitivity of the release process.

Next, because the rate of SV replenishment has been shown to be a critical determinant of asynchronous release (Otsu et al., 2004), we measured the rate at which SVs were replenished following the sucrose-induced depletion by analyzing the steady-state component of the current response. Surprisingly, the rate constant for vesicle replenishment was significantly increased in Raptor-KO neurons compared with that of Raptor-Con neurons (Con: 0.103 ± 0.010 s^{-1}, Rap-KO: 0.179 ± 0.017 s^{-1}, $p < 0.001$; Figure $8A_1$ and $8A_3$), while Rictor-KO did not alter the rate of vesicle replenishment (Con: 0.091 ± 0.013 s^{-1}, Ric-KO: 0.117 ± 0.017 s^{-1}, $p < 0.32$; Figure $8B_1$ and $8B_3$).

535 Finally, to summarize the effects of mTORC1 and mTORC2 inactivation on SV release rates over
536 the range of conditions tested, we plotted the relative changes in rate constants for each of the
537 conditions from lowest to highest rates, plus sucrose (Figure 8C). Taken together, the data indicate that
538 mTORC1 inhibition elevates rate constants for SV fusion under conditions in which the rate is relatively
539 low, but does not affect the rate of fusion when it is high. In contrast, mTORC2 inhibition impairs SV
540 fusion over a wider range of rates, but the effect is more pronounced when rates of SV fusion are high.

Figure 8

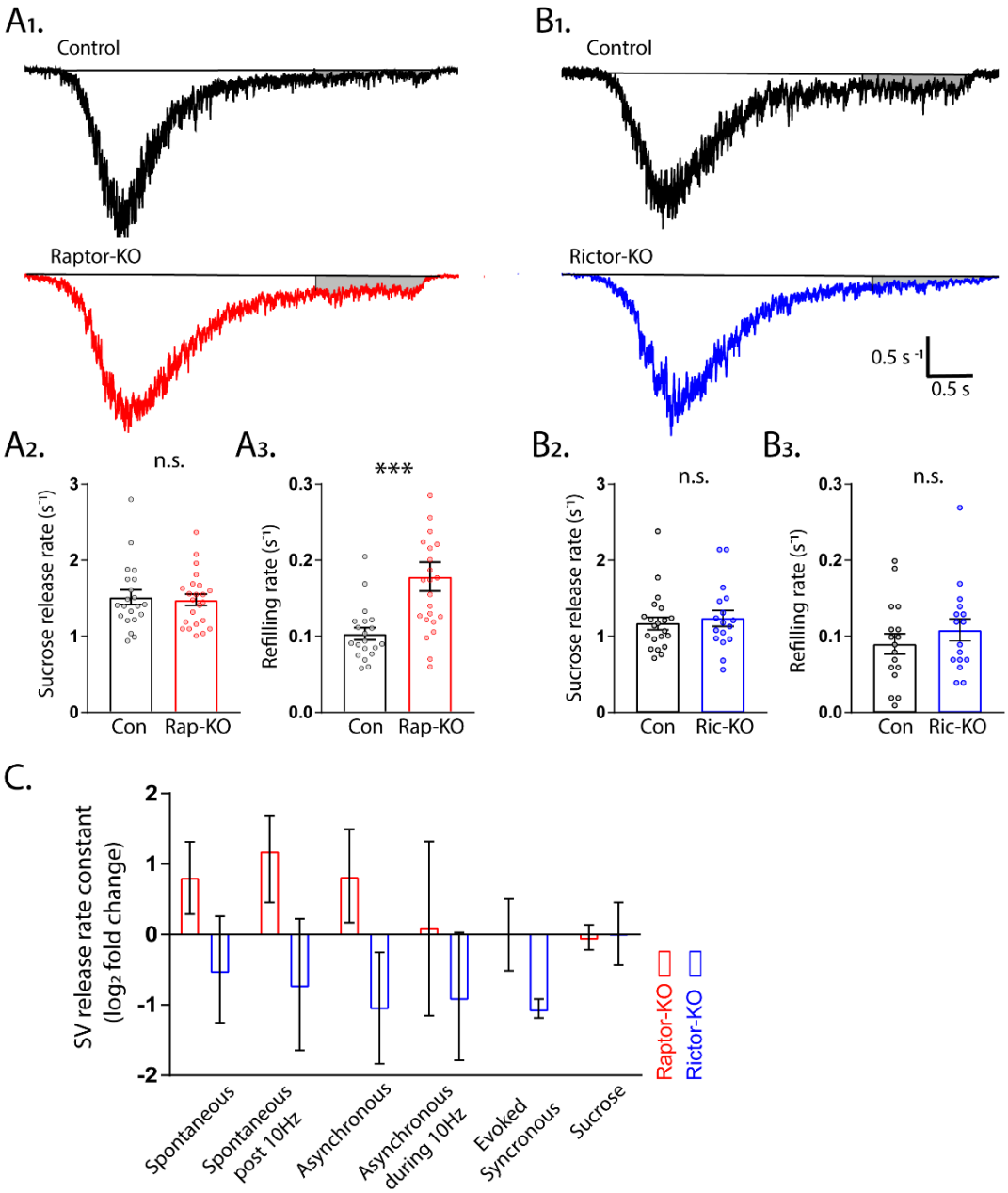

Figure 8. mTOR inactivation does not affect sucrose-induced SV release rates. A_1. Example traces of normalized current responses to 500 mM sucrose application in Raptor-Con (black) and Raptor-KO (red) neurons. The black line shows the pre-sucrose baseline, and the gray shaded area shows the area used to calculate the refilling rate. A_2. Plot showing the rate constants for sucrose-induced synaptic vesicle (SV) release in Raptor-Con (black) and Raptor-KO (red) neurons. A_3. Plot showing the refilling rate constants after sucrose-induced SV release in Raptor-Con (black) and Raptor-KO (red) neurons. B_1. Example traces of normalized current responses to 500 mM sucrose application in Rictor-Con (black) and Rictor-KO (blue) neurons. The black line shows the pre-sucrose baseline, and the gray shaded area shows the area used to calculate the refilling rate. B_2. Plot showing the rate constants for sucrose-induced SV release in Rictor-Con (black) and Rictor-KO (blue) neurons. B_3. Plot showing the refilling rate constants after sucrose-induced SV release in Rictor-Con (black) and Rictor-KO (blue) neurons. C. Plot showing the release rate constants for both Raptor-KO (red) and Rictor-KO (blue) neurons over the range of conditions tested in the study. Each bar represents the mean log2 fold change for that genotype to illustrate the relatively stronger effect of mTORC1 inactivation in potentiating SV release when the rate is low, and of mTORC2 inactivation when the rate is high. Error bars are 95% Confidence Intervals. *** = $p < 0.001$, and n.s. = $p > 0.05$, as tested with Generalized Estimating Equations.

Discussion

Both the mTORC1 and mTORC2 complexes have been shown to regulate important processes such as learning and memory, the response to drugs of abuse, and the development of epilepsy and autism via changes in synaptic strength (Graber, McCamphill, & Sossin, 2013; Hou & Klann, 2004; Huang et al., 2013; Mazei-Robison et al., 2011; Stoica et al., 2011; S. J. Tang et al., 2002). However, the mechanisms underlying the complex-specific changes in synaptic function are largely unknown. Using genetic mouse models to specifically inactivate mTORC1 or mTORC2, and neuronal culture systems to isolate effects, we show here that both complexes are necessary to support normal neuron growth. Previous studies investigating the specific roles of mTORC1 versus mTORC2 in neurons found that inhibiting either complex via shRNA knockdown of *Raptor* or *Rictor* mRNA in hippocampal neurons (Urbanska et al., 2012), or genetic deletion of *Raptor* or *Rictor* in Purkinje neurons (Angliker et al., 2015; Thomanetz et al., 2013), reduced somatic and dendritic growth. In agreement with these studies, we found reductions in neuronal soma size and dendritic length (Figure 1), and corresponding changes in passive membrane properties (Table 1), in both Raptor-KO and Rictor-KO neurons, verifying the general role of both mTORC1 and mTORC2 as regulators of neuron growth.

Because of the high level of crosstalk between the two mTOR-containing complexes (Xie & Proud, 2014), and because of their similar effects on gross neuronal morphology, it is somewhat surprising that their effects on synaptic transmission are non-overlapping and, in some cases, opposite (Figures 7A and 7B). Although inactivation of either complex strongly reduced eEPSC amplitude, we found that the physiological mechanisms underlying these reductions were different, with mTORC1 inhibition reducing eEPSC size via postsynaptic mechanisms and mTORC2 inactivation reducing it through presynaptic mechanisms. Furthermore, we found that mTORC1 inhibition simultaneously increased spontaneous and asynchronous SV release, whereas mTORC2 inhibition decreased evoked and asynchronous SV release. Thus, the roles of mTORC1 and mTORC2 in regulating synaptic

590 transmission are non-overlapping and dissociable from their more general control of neuron growth.
591 Previous studies have shown that synaptic plasticity changes caused by mTOR hyperactivation (PTEN
592 loss) precede large-scale morphological changes (Sperow et al., 2012; Takeuchi et al., 2013), supporting
593 the idea that synaptic transmission and neuron morphology are independently regulated by mTOR.
594 Raptor-KO decreased evoked glutamatergic synaptic transmission (Figure 2), and postsynaptic
595 Raptor-KO was sufficient to cause this decrease (Figure 5). Furthermore, reductions in both the mEPSC
596 amplitude and number of synapses accompanied this decrease (Figure 2). Previous studies showed that
597 mTOR inhibition by rapamycin treatment reduces the number of AMPA receptors at the synapse (Wang
598 et al., 2006), the number of synapses (Weston et al., 2012), and the number of SVs per synapse
599 (Hernandez et al., 2012). Accordingly, mTOR hyperactivation increases mEPSC amplitude (Xiong, Oviedo,
600 Trotman, & Zador, 2012), AMPA receptor number, and spine density (G. Tang et al., 2014; Williams,
601 DeSpenza, Li, Gulledge, & Luikart, 2015), and these effects are blocked by rapamycin. Thus, integrating
602 our findings on specific mTORC1 inactivation with these previous findings, several lines of evidence now
603 indicate that mTORC1 acts via a postsynaptic mechanism to bidirectionally regulate evoked
604 glutamatergic synaptic strength. In contrast to mTORC1 inactivation, mTORC2 inactivation affected
605 presynaptic parameters including P_{vr}, peak evoked SV release rate, and paired pulse ratios, suggesting
606 that the major mechanism through which mTORC2 inactivation reduces eEPSC strength is by impairing
607 presynaptic function. Although neurophysiological deficits have been previously reported in Rictor-KO
608 animals, presynaptic function was not specifically assessed (Dadalko et al., 2015; Huang et al., 2013;
609 Thomanetz et al., 2013; Zhu, Chen, Mays, Stoica, & Costa-Mattioli, 2018). Thus, our data establish
610 mTORC2 as a potent regulator of presynaptic function and suggest that at least some of the previously
611 reported effects of Rictor loss on synaptic transmission are due to presynaptic deficits.
612 The different effects following mTORC1 and mTORC2 inactivation on post- and presynaptic
613 function leads to the question of what downstream targets of each complex mediate these changes. Of

the molecules downstream of mTORC1, 4E-BP, which is inhibited by active mTORC1, is most strongly linked to regulation of synaptic function. In particular, 4E-BP regulates synaptic transmission via its translational repression of the AMPA receptor subunits GluA1 and GluA2 (Ran et al., 2013), and postsynaptic 4E-BP has been shown to play a role in retrograde or trans-synaptic regulation of presynaptic release (Kauwe et al., 2016); thus, the effects of Raptor loss could reflect a combination of these effects. Regarding the presynaptic effects of mTORC2, Akt and PKC isoforms are the most well studied substrates. Although Akt has been suggested to play a role in SV endocytosis (Smillie & Cousin, 2012), multiple PKC isoforms are targets of mTORC2 (Ikenoue, Inoki, Yang, Zhou, & Guan, 2008), and these isoforms are known to influence the RRP, PPRs, asynchronous release, and post-tetanic-potentiation via presynaptic mechanisms (Chang & Mennerick, 2010; Chu, Fioravante, Leitges, & Regehr, 2014; Hori, Takai, & Takahashi, 1999; Xu, Liu, & Alkon, 2014). More specifically, PKC has been shown to regulate the activity of key presynaptic molecules such as Munc-18 (Barclay et al., 2003; Fujita et al., 1996) and Munc-13 (Hori et al., 1999), as well as the actin cytoskeleton (Angliker & Ruegg, 2013). Therefore, the effects of Rictor loss on presynaptic neurotransmission may be caused by lack of PKC activity in these neurons.

Although mTORC1 inactivation decreased evoked strength via postsynaptic mechanisms, it increased the rate of spontaneous and asynchronous release. Because these release rate constants reflect the likelihood of an individual SV to fuse in a given circumstance, they likely reflect a change in the presynaptic terminal. An open question, however, is whether it is reduced mTORC1 activity in the presynapse that causes this change, or whether mTORC1 inactivation in the postsynapse provides a retrograde signal to the presynaptic terminal to alter SV release. In *Drosophila*, 4eBP translationally represses the synaptic protein Complexin to regulate neurotransmitter release at the presynapse (Mahoney, Azpurua, & Eaton, 2016), however, it is not known if this mechanism is conserved, or if it occurs downstream of the mTOR pathway, in mammals. Another mTORC1 target, SREBP1, regulates

cholesterol biosynthesis, and cholesterol depletion has been shown to decrease evoked neurotransmission and enhance spontaneous transmission (Wasser et al., 2007), suggesting that this pathway may mediate the effects on presynaptic release in Raptor-KO neurons. However, as mentioned above, there is evidence that postsynaptic mTOR can signal retrogradely to enhance the RRP and presynaptic release in response to a reduction in postsynaptic glutamate receptor activity (Henry et al., 2012; Henry et al., 2018; Penney et al., 2012), providing proof of principle that mTOR can signal across the synapse. In these studies, mTORC1 *activation* signals to increase the RRP, whereas we found that mTORC1 *inactivation* decreases the RRP, and concomitantly increases the spontaneous and asynchronous SV fusion rates. It is possible that mTORC1 regulates additional trans-synaptic signals that regulate spontaneous and asynchronous release, or that the effect on these release modes is merely compensatory downstream of the reduced evoked transmission, but we think the latter scenario is unlikely because 12 h rapamycin treatment increased spontaneous release, but does not reduce evoked release or synapse number (Weston et al., 2012). Thus, future studies must establish the pre- or postsynaptic locus of the effect of mTORC1 activity on SV release.

One caveat to our findings is that we used the RRP as defined by application of hypertonic sucrose to calculate the rate constants for spontaneous and asynchronous SV fusion. Our analysis assumes that evoked, spontaneous, and asynchronous release all draw from this pool of vesicles. Although there is good evidence to support this assumption (Ryan, Reuter, & Smith, 1997; Schneggenburger & Rosenmund, 2015), it is possible that molecularly distinct SV pools are not all released by sucrose application (Chamberland & Toth, 2016; Fredj & Burrone, 2009; Sara, Virmani, Deak, Liu, & Kavalali, 2005). If true, this may change our specific conclusion that the rate constant of SV fusion changes to the conclusion that the vesicle pools that support evoked, spontaneous, and asynchronous release are differentially affected by the reduction in synapse number caused by Raptor loss. Thus, although our data cannot conclusively distinguish between these two possibilities, the finding that

mTORC1 inactivation enhances asynchronous release after a single stimulation but not after 10 Hz stimulation suggests that it is the SV fusion rate that is affected. We speculate that the differential regulation of SV release modes is due to either the alteration of the sensitivity of SV fusion to calcium (Nosyreva & Kavalali, 2010), or an alteration in the influx of calcium under different conditions, which has been shown to differentially regulate spontaneous and evoked release in response to loss of Presenilin 1 (Pratt, Zhu, Watari, Cook, & Sullivan, 2011). The fact that we found no changes in the sucrose-evoked SV release rate (Figure 8), which is thought to be calcium-independent (Rosenmund & Stevens, 1996), supports the idea that the changes we found are calcium-dependent.

Several recent studies have highlighted instances in which spontaneous and evoked release are independently modified (Ramirez & Kavalali, 2011). It is noteworthy that these examples include blockade of IGF-1 receptors (Gazit et al., 2016), inhibition of protein synthesis (Scarnati et al., 2018), and reduction of cholesterol levels in neurons (Wasser et al., 2007; Zamir & Charlton, 2006), as these are all factors that either feed into mTORC1 activity or are modulated by mTORC1 (Peterson et al., 2011; Saxton & Sabatini, 2017). Because mTORC1 is considered a “hub” that integrates multiple extra- and intracellular cues to control anabolism in cells (J. Kim & Guan, 2019), it is uniquely positioned to coordinate a synaptic response to metabolic changes. Our findings add to a growing body of literature demonstrating that the metabolic state of neurons can signal to synapses to adjust the balance of spontaneous and evoked release (Gazit et al., 2016; Scarnati et al., 2018), and identify a novel role for the mTOR signaling network in maintaining this balance. Furthermore, our data broaden the idea of differential regulation of evoked versus spontaneous release by showing that asynchronous release is also affected. Thus, metabolic changes are not mediating a “competition” or specific ratio between spontaneous and evoked SV release, but instead inducing a shift in the way that synapses respond to different levels of activity, including inactivity.

Variants in at least 10 genes in the mTOR signaling network, including *MTOR*, are known to cause epilepsy, autism, and intellectual disability. Although all of these variants are believed to increase signaling through mTORC1, some have been shown to increase mTORC2 signaling (e.g. *PTEN*, *PIK3CA, and MTOR*), wheras others decrease mTORC2 signaling (e.g. *TSC1*, *TSC2*, and *DEPDC5*). Our data suggest that differential activity levels of the two complexes in disease states would lead to distinct synaptic alterations. Accordingly, previous studies have shown that *Pten* loss and *Tsc1* loss cause different synaptic alterations (Bateup et al., 2013; Chamberland & Toth, 2016; Williams et al., 2015). Together, these data suggest that complex specific targeting may be necessary to restore normal synaptic function in neurological diseases involving mTOR hyperactivation. Moreover, future studies are needed to further clarify the contributions of each mTOR complex to these neurological diseases.

Materials and Methods

Mice and cell culture

Animal housing and use were in compliance with the National Institutes of Health (NIH) Guidelines for the Care and Use of Laboratory Animals and were approved by the Institutional Animal Care and Use Committee at the University of Vermont. Experiments used B6.Cg-*Rptor*$^{tm1.1Dmsa}$/J mice that possess loxP sites on either side of exon 6 of the *Raptor* gene (Jackson Labs stock: 013188), *Rictor*$^{tm1.1Klg}$/SjmJ mice that possess loxP sites on either side of exon 11 of the *Rictor* gene (Jackson Labs stock: 020649), and *Tsc1*^{tm1Djk}/J mice that possess loxP sites around exons 17 and 18 of the *Tsc1* gene (Jackson Labs stock: 005680). All three lines were maintained as homozygous for the floxed allele. Experiments that involved treatment of wild-type neuronal cultures with drugs used C57BL/6J mice (Jackson Labs stock: 000664).

Conventional and single-neuron primary cultures were grown on astrocytes derived from wild-type C57BL/6J mice (Jackson Labs stock: 000664). Cortices were dissected from postnatal day 0-1 (P0-

P1) mice of either sex and placed in 0.05% trypsin-EDTA (Gibco) for 15 min at 37°C in a Thermomixer (Eppendorf) with gentle agitation (800 rpm). Then, the cortices were mechanically dissociated with a 1 mL pipette tip and the cells were plated into T-75 flasks containing astrocyte media [DMEM media supplemented with glutamine (Gibco) and MITO+ Serum Extender (Corning). After the astrocytes reached confluency, they were washed with PBS (Gibco) and incubated for 5 min in 0.05% trypsin-EDTA at 37°C, and then resuspended in astrocyte media. For conventional cultures, the astrocytes were added to 6-well plates containing 25-mm coverslips precoated with coating mixture [0.7 mg/ml collagen I (Corning) and 0.1 mg/ml poly-D-lysine (Sigma) in 10 mM acetic acid]. For single-neuron cultures, the astrocytes were added to 6-well plates containing 25-mm agarose-coated coverslips stamped with coating mixture using a custom-built stamp to achieve uniformly sized, astrocyte microislands (200-µm diameter).

For the primary neuron culture, the hippocampi from P0-P1 mice of both sexes were dissected in cold HBSS (Gibco). The hippocampi were then digested with papain (Worthington) for 60-75 min and treated with inactivating solution (Worthington) for 10 min, both while shaking at 800 rpm at 37°C in a Thermomixer. The neurons were then mechanically dissociated and counted. For single-neuron cultures, 2000-3000 neurons/well were added to 6-well plates in NBA plus [Neurobasal-A medium (Gibco) supplemented with Glutamax (Gibco) and B27 (Invitrogen)], each well containing a 25-mm coverslip with astrocyte microislands. For conventional cultures, 150,000 neurons/well were added to 6-well plates in NBA plus, each well containing a 25-mm coverslip with a confluent layer of astrocytes. After plating, approximately 4×10^{10} genome copies (GC) of either AAV8-hsyn-mCherry-Cre or AAV8-hsyn-mCherry virus (UNC Vector Core) was added to each well. For the treatment of WT neurons with rapamycin experiment, rapamycin (Cayman Chemical) was dissolved in DMSO at a concentration of 20 µM and then added to cell culture media at a 1:1000 dilution for 12-16 hr prior to electrophysiology

732 experiments to achieve a final concentration of 20 nM. Control neurons were treated with an equal
733 amount of DMSO alone.
734 For experiments using paired recording and optogenetic excitation, the neuron suspensions
735 after hippocampal dissociation were split into three tubes of 300 µl each. To one of these tubes, 6×10^{10}
736 GC of AAV8-hsyn-mCherry-Cre was added, and to another, 6×10^{10} GC of AAV9-Syn-Chronos-
737 GFP(Klapoetke et al., 2014) was added. The virus was left on for 3 hr while the neuron suspensions were
738 gently shaken (500 rpm) at 37°C in a Thermomixer. After 3 hr, the neurons were centrifuged three times
739 at 1500 rpm for 5 min on a benchtop centrifuge and resuspended in fresh Neurobasal-A medium each
740 time. After the third resuspension, the neurons were counted. From each of the three tubes, 50,000
741 neurons were added to each well of a 6-well plate containing NBA plus to generate a network containing
742 Control, Cre-expressing, and Chronos-expressing neurons in non-overlapping neuronal population.
743 **Immunocytochemistry**
744 Neurons were rinsed three times with PBS, fixed with 4% PFA for 30 min, and then washed with
745 PBS three times. Neurons were then placed in blocking solution (10% NGS, 0.1% Triton X-100, and PBS)
746 at room temperature for 1 hr. The following primary antibodies in blocking solution were then applied
747 to the neurons at 4°C overnight: MAP2 (mouse monoclonal, 1:1000 dilution, Synaptic Systems, Cat# 188
748 011, RRID:AB_2147096), phospho-S6 Ribosomal Protein Ser240/244 (rabbit monoclonal, 1:1000 dilution,
749 Cell Signaling Technology, Cat# 5364, RRID:AB_10694233), phospho-AKT Ser473 (rabbit monoclonal,
750 1:1000 dilution, Cell Signaling Technology, Cat# 4060, RRID:AB_2315049), and VGLUT1 (rabbit
751 polyclonal, 1:5000 dilution, Synaptic Systems, Cat # 135 302, RRID:AB_887877). Following primary
752 antibody application, cells were washed three times in PBS and then incubated in the following Alexa
753 Fluor secondary antibodies (Invitrogen/Molecular Probes) for 1 hr at room temperature: goat anti-
754 mouse 488 (1:1000, Cat # A-11017, RRID:AB_143160) and goat anti-rabbit 647 (1:1000, Cat# A-21244,

RRID:AB_141663). Cells were then mounted to slides with Prolong Gold Antifade (Life Technologies) and allowed to cure for 24 hr.

Images (1024 × 1024 pixels) for pS6 and pAKT expression analysis were obtained using a DeltaVision Restoration Microscopy System (Applied Precision/GE Life Sciences) with an inverted Olympus IX70 microscope with a 20× oil objective, SoftWoRx software, and a CoolSNAP-HQ charge-coupled device digital camera (Photometrics). Image exposure times and settings were kept the same between groups in a culture and were optimized to ensure that there were no saturated pixels. Images were acquired in stacks of 8–12 planes at 0.5 µm depth intervals and then deconvolved. Stacks were processed using Fiji software (Schindelin et al., 2012) to create maximum intensity projections. Image background was subtracted using the rolling ball method with a radius of 100 µm. To analyze levels of mTOR effectors, regions of interest (ROIs) were drawn around the cell body using the MAP2 channel, and then the mean fluorescence intensity and cell body area were measured for pS6 and pAKT for each neuron imaged. Because the absolute values of the fluorescence intensity varied between cultures, the values were normalized to the mean value of the control neurons for each culture.

For dendritic length and glutamatergic terminal number analysis, primary neuron cultures on astrocyte microislands were generated and fixed as described above. Images (1024 x 1024 pixels) were obtained using a C2 confocal microscopy system (Nikon) with a 40x oil objective. Images were acquired using equal exposure times between groups in stacks of 4-6 images at 2.0 µm depth intervals. Maximum intensity projections were created using Fiji software. Total dendritic length was obtained by tracing MAP2 expression using the NeuronJ plugin (Meijering et al., 2004). VGLUT puncta number was calculated using Intellicount software (Fantuzzo et al., 2017).

Electrophysiology

778 Whole-cell recordings were performed with patch-clamp amplifiers (MultiClamp 700B amplifier;
779 Molecular Devices) under the control of Clampex 10.3 or 10.5 (Molecular Devices, pClamp,
780 RRID:SCR_011323). Data were acquired at 10 kHz and low-pass filtered at 6 kHz. The series resistance
781 was compensated at 70%, and only cells with series resistances maintained at less than 15 MΩ were
782 analyzed. The pipette resistance was between 2 and 4 MΩ. Standard extracellular solution contained the
783 following (in mM): 140 NaCl, 2.4 KCl, 10 HEPES, 10 glucose, 4 $MgCl_2$, and 2 $CaCl_2$ (pH 7.3, 305 mOsm).
784 Internal solution contained the following: 136 mM K-gluconate, 17.8 mM HEPES, 1 mM EGTA, 0.6 mM
785 $MgCl_2$, 4 mM ATP, 0.3 mM GTP, 12 mM creatine phosphate, and 50 U/ml phosphocreatine kinase. All
786 experiments were performed at room temperature (22–23°C). Whole-cell recordings were performed
787 on neurons from control and mutant groups in parallel on the same day (day 12–14 *in vitro*).
788 For voltage-clamp experiments, neurons were held at -70 mV unless noted. Action potential
789 (AP)-evoked EPSCs were triggered by a 2 ms somatic depolarization to 0 mV. The shape of the evoked
790 response and the effect of receptor antagonists [3 mM kynurenic acid (KYN, Tocris Bioscience) or 20 µM
791 bicuculline (BIC, Tocris Bioscience)] were analyzed to verify the glutamatergic or GABAergic identities of
792 the neurons. Neurons were stimulated at 0.2 Hz in standard external solution to measure basal-evoked
793 synaptic responses. Electrophysiology data were analyzed offline with AxoGraph X software (AxoGraph
794 Scientific, RRID:SCR_014284). To determine the number of releasable SVs onto each neuron, we
795 measured the charge transfer of the transient synaptic current induced by a 5 s application of
796 hypertonic sucrose solution directly onto the neuron and then divided the sucrose charge by the charge
797 of the average miniature event onto the same neuron (Rosenmund & Stevens, 1996).
798 For current-clamp experiments, the resting membrane potential was measured and then
799 current was injected to achieve a resting membrane potential of -70 mV. KYN was applied to block
800 synaptic responses. Input resistance and membrane time constant were calculated from the steady
801 state and charging transient, respectively, of voltage responses to 0.5 s, 20 pA hyperpolarizing current

steps. Membrane capacitance was calculated by dividing the time constant by the input resistance. AP were evoked with 0.5 s, 20 pA depolarizing current steps. AP threshold was defined as the membrane potential at the inflection point of the rising phase of the AP. AP amplitude was defined as the difference in membrane potential between the AP peak and threshold. The membrane potential values were not corrected for the liquid junction potential.

Miniature event detection

Miniature synaptic potentials were recorded for 70–90 s in 500 nM tetrodotoxin (TTX, Enzo Life Sciences) to block AP-evoked release. Data were filtered at 1 kHz and analyzed using template-based miniature event detection algorithms implemented in the AxoGraph X. The threshold for detection was set at three times the baseline SD from a template of 0.5 ms rise time and 3 ms decay. For each neuron, 3 mM KYN was applied as a negative control to detect false positive events. If the frequency of false positives exceeded 0.25 the frequency of total positives, the neuron was discarded. If rate was lower than 0.25, the amplitude and frequency of false positives were subtracted from the total to obtain the rate and frequency of true positives.

Synaptic vesicle release rate analysis

The rate constant for vesicle fusion (k) was calculated for each neuron and each mode of vesicle release with the first order reaction equation r = k [A], where r = the observed vesicle release rate (SVs/s) and A = the number of SVs in the RRP. For spontaneous release, the observed vesicle release rate was the mEPSC frequency. For the peak rate of evoked SV release, at least 10 EPSCs were collected per neuron, baselined to the 5 ms period immediately preceding the stimulation, filtered at 1 kHz and deconvolved with the waveform of the mean mEPSC from that neuron using a custom algorithm implemented in Axograph X to give the SV release rate waveform. The deconvolved EPSC waveform was

826 then integrated and the maximum slope over a 1 ms time bin was considered the peak rate of SV
827 release. For the spontaneous release rate after 10 Hz stimulation, the vesicle release rate was the mean
828 mEPSC frequency over 10 s beginning 100 ms after the last stimulation in the train. For asynchronous
829 release, the vesicle release rate was calculated by fitting a single exponential to the fast component of
830 the EPSC decay, subtracting the fast component from the total, and then dividing the charge transfer of
831 the remaining response by the charge of the average mEPSC for each neuron. For asynchronous release
832 during 10 Hz stimulation, the vesicle release rate was calculated by baselining the first EPSC in the train,
833 fitting a single exponential to the fast component of the EPSC decay of the last EPSC in the train,
834 subtracting the fast component from the total, and then dividing the charge transfer of the remaining
835 response by the charge of the average mEPSC for each neuron (Chang & Mennerick, 2010; Otsu et al.,
836 2004). To account for depletion of the pool during the train, A was estimated by multiplying the number
837 of SVs in the RRP times the ratio of the charge of the last EPSC to the charge of the first EPSC in the train.
838 Although we note that this may underestimate the amount of depletion due to an increase in release
839 probability during the train.
840
841 **Experimental design and statistical analysis**
842 KaleidaGraph 4.5 (Synergy Software) and Prism 7 (GraphPad Prism, RRID:SCR_002798) were
843 used to create graphs. To test for statistical significance, we used generalized estimating equations (GEE)
844 in SPSS (24.0 Chicago, III (IBM, RRID:SCR_002865), which allows for within-subject correlations and the
845 specification of the most appropriate distribution for the data. All data distributions were assessed with
846 the Shapiro-Wilk test. Datasets that were significantly different from the normal distribution ($p < 0.05$)
847 were fit with models using the gamma distribution and a log link. Normal datasets were fit with models
848 using a linear distribution and identity link. We used the model-based estimator for the covariance
849 matrix and an exchangeable structure for the working correlation matrix. Goodness of fit was

850 determined using the corrected quasi likelihood under independence model criterion and by the visual
851 assessment of residuals. Because neurons and animals from the same culture are not independent
852 measurements, culture was used as the subject variable, and animals and neurons were considered
853 within-subject measurements. All values reported in the text are estimated marginal means +/- standard
854 error. To determine our sample size for the experiments using paired recording and optogenetic
855 excitation, we performed a power analysis based on the EPSC amplitude measurements in the single-
856 neuron cultures and calculated the number of pairs we needed to record from to detect a difference
857 with 80% power at $\alpha = 0.05$ in each group if the effect on EPSC amplitude were purely postsynaptic.
858
859
860
861
862
863
864
865
866
867
868
869
870
871
872
873

References

Angliker, N., Burri, M., Zaichuk, M., Fritschy, J. M., & Ruegg, M. A. (2015). mTORC1 and mTORC2 have largely distinct functions in Purkinje cells. *Eur J Neurosci, 42*(8), 2595-2612. doi:10.1111/ejn.13051

Angliker, N., & Ruegg, M. A. (2013). In vivo evidence for mTORC2-mediated actin cytoskeleton rearrangement in neurons. *Bioarchitecture, 3*(4), 113-118. doi:10.4161/bioa.26497

Aumann, Y., & Parnas, H. (1991). Evaluation of the time course of neurotransmitter release from the measured PSC and MPSC. *Bull Math Biol, 53*(4), 537-555.

Barclay, J. W., Craig, T. J., Fisher, R. J., Ciufo, L. F., Evans, G. J., Morgan, A., & Burgoyne, R. D. (2003). Phosphorylation of Munc18 by protein kinase C regulates the kinetics of exocytosis. *J Biol Chem, 278*(12), 10538-10545. doi:10.1074/jbc.M211114200

Basu, J., Betz, A., Brose, N., & Rosenmund, C. (2007). Munc13-1 C1 domain activation lowers the energy barrier for synaptic vesicle fusion. *J Neurosci, 27*(5), 1200-1210. doi:10.1523/JNEUROSCI.4908-06.2007

Bateup, H. S., Johnson, C. A., Denefrio, C. L., Saulnier, J. L., Kornacker, K., & Sabatini, B. L. (2013). Excitatory/inhibitory synaptic imbalance leads to hippocampal hyperexcitability in mouse models of tuberous sclerosis. *Neuron, 78*(3), 510-522. doi:10.1016/j.neuron.2013.03.017

Chamberland, S., & Toth, K. (2016). Functionally heterogeneous synaptic vesicle pools support diverse synaptic signalling. *J Physiol, 594*(4), 825-835. doi:10.1113/JP270194

Chang, C. Y., & Mennerick, S. (2010). Dynamic modulation of phasic and asynchronous glutamate release in hippocampal synapses. *J Neurophysiol, 103*(1), 392-401. doi:10.1152/jn.00683.2009

Chu, Y., Fioravante, D., Leitges, M., & Regehr, W. G. (2014). Calcium-dependent PKC isoforms have specialized roles in short-term synaptic plasticity. *Neuron, 82*(4), 859-871. doi:10.1016/j.neuron.2014.04.003

Crino, P. B. (2011). mTOR: A pathogenic signaling pathway in developmental brain malformations. *Trends Mol Med, 17*(12), 734-742. doi:10.1016/j.molmed.2011.07.008

Dadalko, O. I., Siuta, M., Poe, A., Erreger, K., Matthies, H. J., Niswender, K., & Galli, A. (2015). mTORC2/rictor signaling disrupts dopamine-dependent behaviors via defects in striatal dopamine neurotransmission. *J Neurosci, 35*(23), 8843-8854. doi:10.1523/JNEUROSCI.0887-15.2015

Diamond, J. S., & Jahr, C. E. (1995). Asynchronous release of synaptic vesicles determines the time course of the AMPA receptor-mediated EPSC. *Neuron, 15*(5), 1097-1107.

Edinger, A. L., & Thompson, C. B. (2002). Akt maintains cell size and survival by increasing mTOR-dependent nutrient uptake. *Mol Biol Cell, 13*(7), 2276-2288. doi:10.1091/mbc.01-12-0584

Fantuzzo, J. A., Mirabella, V. R., Hamod, A. H., Hart, R. P., Zahn, J. D., & Pang, Z. P. (2017). Intellicount: High-Throughput Quantification of Fluorescent Synaptic Protein Puncta by Machine Learning. *eNeuro, 4*(6). doi:10.1523/ENEURO.0219-17.2017

Fredj, N. B., & Burrone, J. (2009). A resting pool of vesicles is responsible for spontaneous vesicle fusion at the synapse. *Nat Neurosci, 12*(6), 751-758. doi:10.1038/nn.2317

Fujita, Y., Sasaki, T., Fukui, K., Kotani, H., Kimura, T., Hata, Y., . . . Takai, Y. (1996). Phosphorylation of Munc-18/n-Sec1/rbSec1 by protein kinase C: its implication in regulating the interaction of Munc-18/n-Sec1/rbSec1 with syntaxin. *J Biol Chem, 271*(13), 7265-7268. doi:10.1074/jbc.271.13.7265

Gazit, N., Vertkin, I., Shapira, I., Helm, M., Slomowitz, E., Sheiba, M., . . . Slutsky, I. (2016). IGF-1 Receptor Differentially Regulates Spontaneous and Evoked Transmission via Mitochondria at Hippocampal Synapses. *Neuron, 89*(3), 583-597. doi:10.1016/j.neuron.2015.12.034

Graber, T. E., McCamphill, P. K., & Sossin, W. S. (2013). A recollection of mTOR signaling in learning and memory. *Learn Mem, 20*(10), 518-530. doi:10.1101/lm.027664.112

Hay, N., & Sonenberg, N. (2004). Upstream and downstream of mTOR. *Genes Dev, 18*(16), 1926-1945. doi:10.1101/gad.1212704

Henry, F. E., McCartney, A. J., Neely, R., Perez, A. S., Carruthers, C. J., Stuenkel, E. L., . . . Sutton, M. A. (2012). Retrograde changes in presynaptic function driven by dendritic mTORC1. *J Neurosci, 32*(48), 17128-17142. doi:10.1523/JNEUROSCI.2149-12.2012

Henry, F. E., Wang, X., Serrano, D., Perez, A. S., Carruthers, C. J. L., Stuenkel, E. L., & Sutton, M. A. (2018). A Unique Homeostatic Signaling Pathway Links Synaptic Inactivity to Postsynaptic mTORC1. *J Neurosci, 38*(9), 2207-2225. doi:10.1523/JNEUROSCI.1843-17.2017

Hernandez, D., Torres, C. A., Setlik, W., Cebrian, C., Mosharov, E. V., Tang, G., . . . Sulzer, D. (2012). Regulation of presynaptic neurotransmission by macroautophagy. *Neuron, 74*(2), 277-284. doi:10.1016/j.neuron.2012.02.020

Hori, T., Takai, Y., & Takahashi, T. (1999). Presynaptic mechanism for phorbol ester-induced synaptic potentiation. *J Neurosci, 19*(17), 7262-7267.

Hou, L., & Klann, E. (2004). Activation of the phosphoinositide 3-kinase-Akt-mammalian target of rapamycin signaling pathway is required for metabotropic glutamate receptor-dependent long-term depression. *J Neurosci, 24*(28), 6352-6361. doi:10.1523/JNEUROSCI.0995-04.2004

Hsu, P. P., Kang, S. A., Rameseder, J., Zhang, Y., Ottina, K. A., Lim, D., . . . Sabatini, D. M. (2011). The mTOR-regulated phosphoproteome reveals a mechanism of mTORC1-mediated inhibition of growth factor signaling. *Science, 332*(6035), 1317-1322. doi:10.1126/science.1199498

Huang, W., Zhu, P. J., Zhang, S., Zhou, H., Stoica, L., Galiano, M., . . . Costa-Mattioli, M. (2013). mTORC2 controls actin polymerization required for consolidation of long-term memory. *Nat Neurosci, 16*(4), 441-448. doi:10.1038/nn.3351

Ikenoue, T., Inoki, K., Yang, Q., Zhou, X., & Guan, K. L. (2008). Essential function of TORC2 in PKC and Akt turn motif phosphorylation, maturation and signalling. *EMBO J, 27*(14), 1919-1931. doi:10.1038/emboj.2008.119

Kaeser, P. S., & Regehr, W. G. (2014). Molecular mechanisms for synchronous, asynchronous, and spontaneous neurotransmitter release. *Annu Rev Physiol, 76*, 333-363. doi:10.1146/annurev-physiol-021113-170338

Kang, S. A., Pacold, M. E., Cervantes, C. L., Lim, D., Lou, H. J., Ottina, K., . . . Sabatini, D. M. (2013). mTORC1 phosphorylation sites encode their sensitivity to starvation and rapamycin. *Science, 341*(6144), 1236566. doi:10.1126/science.1236566

Kauwe, G., Tsurudome, K., Penney, J., Mori, M., Gray, L., Calderon, M. R., . . . Haghighi, A. P. (2016). Acute Fasting Regulates Retrograde Synaptic Enhancement through a 4E-BP-Dependent Mechanism. *Neuron, 92*(6), 1204-1212. doi:10.1016/j.neuron.2016.10.063

Kim, D. H., Sarbassov, D. D., Ali, S. M., King, J. E., Latek, R. R., Erdjument-Bromage, H., . . . Sabatini, D. M. (2002). mTOR interacts with raptor to form a nutrient-sensitive complex that signals to the cell growth machinery. *Cell, 110*(2), 163-175.

Kim, J., & Guan, K. L. (2019). mTOR as a central hub of nutrient signalling and cell growth. *Nat Cell Biol, 21*(1), 63-71. doi:10.1038/s41556-018-0205-1

Klapoetke, N. C., Murata, Y., Kim, S. S., Pulver, S. R., Birdsey-Benson, A., Cho, Y. K., . . . Boyden, E. S. (2014). Independent optical excitation of distinct neural populations. *Nat Methods, 11*(3), 338-346. doi:10.1038/nmeth.2836

Lipton, J. O., & Sahin, M. (2014). The neurology of mTOR. *Neuron, 84*(2), 275-291. doi:10.1016/j.neuron.2014.09.034

Mahoney, R. E., Azpurua, J., & Eaton, B. A. (2016). Insulin signaling controls neurotransmission via the 4eBP-dependent modification of the exocytotic machinery. *Elife, 5*. doi:10.7554/eLife.16807

968 Mazei-Robison, M. S., Koo, J. W., Friedman, A. K., Lansink, C. S., Robison, A. J., Vinish, M., . . . Nestler, E.
969 J. (2011). Role for mTOR signaling and neuronal activity in morphine-induced adaptations in
970 ventral tegmental area dopamine neurons. *Neuron, 72*(6), 977-990.
971 doi:10.1016/j.neuron.2011.10.012
972 Meijering, E., Jacob, M., Sarria, J. C., Steiner, P., Hirling, H., & Unser, M. (2004). Design and validation of
973 a tool for neurite tracing and analysis in fluorescence microscopy images. *Cytometry A, 58*(2),
974 167-176. doi:10.1002/cyto.a.20022
975 Niere, F., Namjoshi, S., Song, E., Dilly, G. A., Schoenhard, G., Zemelman, B. V., . . . Raab-Graham, K. F.
976 (2016). Analysis of Proteins That Rapidly Change Upon Mechanistic/Mammalian Target of
977 Rapamycin Complex 1 (mTORC1) Repression Identifies Parkinson Protein 7 (PARK7) as a Novel
978 Protein Aberrantly Expressed in Tuberous Sclerosis Complex (TSC). *Mol Cell Proteomics, 15*(2),
979 426-444. doi:10.1074/mcp.M115.055079
980 Nosyreva, E., & Kavalali, E. T. (2010). Activity-dependent augmentation of spontaneous
981 neurotransmission during endoplasmic reticulum stress. *J Neurosci, 30*(21), 7358-7368.
982 doi:10.1523/JNEUROSCI.5358-09.2010
983 O'Reilly, K. E., Rojo, F., She, Q. B., Solit, D., Mills, G. B., Smith, D., . . . Rosen, N. (2006). mTOR inhibition
984 induces upstream receptor tyrosine kinase signaling and activates Akt. *Cancer Res, 66*(3), 1500-
985 1508. doi:10.1158/0008-5472.CAN-05-2925
986 Otsu, Y., Shahrezaei, V., Li, B., Raymond, L. A., Delaney, K. R., & Murphy, T. H. (2004). Competition
987 between phasic and asynchronous release for recovered synaptic vesicles at developing
988 hippocampal autaptic synapses. *J Neurosci, 24*(2), 420-433. doi:10.1523/JNEUROSCI.4452-
989 03.2004
990 Penney, J., Tsurudome, K., Liao, E. H., Elazzouzi, F., Livingstone, M., Gonzalez, M., . . . Haghighi, A. P.
991 (2012). TOR is required for the retrograde regulation of synaptic homeostasis at the Drosophila
992 neuromuscular junction. *Neuron, 74*(1), 166-178. doi:10.1016/j.neuron.2012.01.030
993 Peterson, T. R., Sengupta, S. S., Harris, T. E., Carmack, A. E., Kang, S. A., Balderas, E., . . . Sabatini, D. M.
994 (2011). mTOR complex 1 regulates lipin 1 localization to control the SREBP pathway. *Cell, 146*(3),
995 408-420. doi:10.1016/j.cell.2011.06.034
996 Pratt, K. G., Zhu, P., Watari, H., Cook, D. G., & Sullivan, J. M. (2011). A novel role for {gamma}-secretase:
997 selective regulation of spontaneous neurotransmitter release from hippocampal neurons. *J*
998 *Neurosci, 31*(3), 899-906. doi:10.1523/JNEUROSCI.4625-10.2011
999 Ramirez, D. M., & Kavalali, E. T. (2011). Differential regulation of spontaneous and evoked
1000 neurotransmitter release at central synapses. *Curr Opin Neurobiol, 21*(2), 275-282.
1001 doi:10.1016/j.conb.2011.01.007
1002 Ran, I., Gkogkas, C. G., Vasuta, C., Tartas, M., Khoutorsky, A., Laplante, I., . . . Lacaille, J. C. (2013).
1003 Selective regulation of GluA subunit synthesis and AMPA receptor-mediated synaptic function
1004 and plasticity by the translation repressor 4E-BP2 in hippocampal pyramidal cells. *J Neurosci,*
1005 *33*(5), 1872-1886. doi:10.1523/JNEUROSCI.3264-12.2013
1006 Rosenmund, C., & Stevens, C. F. (1996). Definition of the readily releasable pool of vesicles at
1007 hippocampal synapses. *Neuron, 16*(6), 1197-1207.
1008 Ryan, T. A., Reuter, H., & Smith, S. J. (1997). Optical detection of a quantal presynaptic membrane
1009 turnover. *Nature, 388*(6641), 478-482. doi:10.1038/41335
1010 Sakaba, T., & Neher, E. (2001). Quantitative relationship between transmitter release and calcium
1011 current at the calyx of held synapse. *J Neurosci, 21*(2), 462-476.
1012 Sara, Y., Virmani, T., Deak, F., Liu, X., & Kavalali, E. T. (2005). An isolated pool of vesicles recycles at rest
1013 and drives spontaneous neurotransmission. *Neuron, 45*(4), 563-573.
1014 doi:10.1016/j.neuron.2004.12.056

Sarbassov, D. D., Ali, S. M., Sengupta, S., Sheen, J. H., Hsu, P. P., Bagley, A. F., . . . Sabatini, D. M. (2006). Prolonged rapamycin treatment inhibits mTORC2 assembly and Akt/PKB. *Mol Cell, 22*(2), 159-168. doi:10.1016/j.molcel.2006.03.029

Saxton, R. A., & Sabatini, D. M. (2017). mTOR Signaling in Growth, Metabolism, and Disease. *Cell, 169*(2), 361-371. doi:10.1016/j.cell.2017.03.035

Scarnati, M. S., Kataria, R., Biswas, M., & Paradiso, K. G. (2018). Active presynaptic ribosomes in the mammalian brain, and altered transmitter release after protein synthesis inhibition. *Elife, 7*. doi:10.7554/eLife.36697

Schindelin, J., Arganda-Carreras, I., Frise, E., Kaynig, V., Longair, M., Pietzsch, T., . . . Cardona, A. (2012). Fiji: an open-source platform for biological-image analysis. *Nat Methods, 9*(7), 676-682. doi:10.1038/nmeth.2019

Schneggenburger, R., & Neher, E. (2000). Intracellular calcium dependence of transmitter release rates at a fast central synapse. *Nature, 406*(6798), 889-893. doi:10.1038/35022702

Schneggenburger, R., & Rosenmund, C. (2015). Molecular mechanisms governing Ca(2+) regulation of evoked and spontaneous release. *Nat Neurosci, 18*(7), 935-941. doi:10.1038/nn.4044

Smillie, K. J., & Cousin, M. A. (2012). Akt/PKB controls the activity-dependent bulk endocytosis of synaptic vesicles. *Traffic, 13*(7), 1004-1011. doi:10.1111/j.1600-0854.2012.01365.x

Sperow, M., Berry, R. B., Bayazitov, I. T., Zhu, G., Baker, S. J., & Zakharenko, S. S. (2012). Phosphatase and tensin homologue (PTEN) regulates synaptic plasticity independently of its effect on neuronal morphology and migration. *J Physiol, 590*(4), 777-792. doi:10.1113/jphysiol.2011.220236

Stoica, L., Zhu, P. J., Huang, W., Zhou, H., Kozma, S. C., & Costa-Mattioli, M. (2011). Selective pharmacogenetic inhibition of mammalian target of Rapamycin complex I (mTORC1) blocks long-term synaptic plasticity and memory storage. *Proc Natl Acad Sci U S A, 108*(9), 3791-3796. doi:10.1073/pnas.1014715108

Sudhof, T. C. (2012). Calcium control of neurotransmitter release. *Cold Spring Harb Perspect Biol, 4*(1), a011353. doi:10.1101/cshperspect.a011353

Takeuchi, K., Gertner, M. J., Zhou, J., Parada, L. F., Bennett, M. V., & Zukin, R. S. (2013). Dysregulation of synaptic plasticity precedes appearance of morphological defects in a Pten conditional knockout mouse model of autism. *Proc Natl Acad Sci U S A, 110*(12), 4738-4743. doi:10.1073/pnas.1222803110

Tang, G., Gudsnuk, K., Kuo, S. H., Cotrina, M. L., Rosoklija, G., Sosunov, A., . . . Sulzer, D. (2014). Loss of mTOR-dependent macroautophagy causes autistic-like synaptic pruning deficits. *Neuron, 83*(5), 1131-1143. doi:10.1016/j.neuron.2014.07.040

Tang, S. J., Reis, G., Kang, H., Gingras, A. C., Sonenberg, N., & Schuman, E. M. (2002). A rapamycin-sensitive signaling pathway contributes to long-term synaptic plasticity in the hippocampus. *Proc Natl Acad Sci U S A, 99*(1), 467-472. doi:10.1073/pnas.012605299

Thomanetz, V., Angliker, N., Cloetta, D., Lustenberger, R. M., Schweighauser, M., Oliveri, F., . . . Ruegg, M. A. (2013). Ablation of the mTORC2 component rictor in brain or Purkinje cells affects size and neuron morphology. *J Cell Biol, 201*(2), 293-308. doi:10.1083/jcb.201205030

Urbanska, M., Gozdz, A., Swiech, L. J., & Jaworski, J. (2012). Mammalian target of rapamycin complex 1 (mTORC1) and 2 (mTORC2) control the dendritic arbor morphology of hippocampal neurons. *J Biol Chem, 287*(36), 30240-30256. doi:10.1074/jbc.M112.374405

Wang, Y., Barbaro, M. F., & Baraban, S. C. (2006). A role for the mTOR pathway in surface expression of AMPA receptors. *Neurosci Lett, 401*(1-2), 35-39. doi:10.1016/j.neulet.2006.03.011

Wasser, C. R., Ertunc, M., Liu, X., & Kavalali, E. T. (2007). Cholesterol-dependent balance between evoked and spontaneous synaptic vesicle recycling. *J Physiol, 579*(Pt 2), 413-429. doi:10.1113/jphysiol.2006.123133

1063 Weston, M. C., Chen, H., & Swann, J. W. (2012). Multiple roles for mammalian target of rapamycin
1064 signaling in both glutamatergic and GABAergic synaptic transmission. *J Neurosci, 32*(33), 11441-
1065 11452. doi:10.1523/JNEUROSCI.1283-12.2012
1066 Weston, M. C., Chen, H., & Swann, J. W. (2014). Loss of mTOR repressors Tsc1 or Pten has divergent
1067 effects on excitatory and inhibitory synaptic transmission in single hippocampal neuron cultures.
1068 *Front Mol Neurosci, 7*, 1. doi:10.3389/fnmol.2014.00001
1069 Williams, M. R., DeSpenza, T., Jr., Li, M., Gulledge, A. T., & Luikart, B. W. (2015). Hyperactivity of
1070 newborn Pten knock-out neurons results from increased excitatory synaptic drive. *J Neurosci,*
1071 *35*(3), 943-959. doi:10.1523/JNEUROSCI.3144-14.2015
1072 Wullschleger, S., Loewith, R., & Hall, M. N. (2006). TOR signaling in growth and metabolism. *Cell, 124*(3),
1073 471-484. doi:10.1016/j.cell.2006.01.016
1074 Xie, J., & Proud, C. G. (2014). Signaling crosstalk between the mTOR complexes. *Translation (Austin),*
1075 *2*(1), e28174. doi:10.4161/trla.28174
1076 Xiong, Q., Oviedo, H. V., Trotman, L. C., & Zador, A. M. (2012). PTEN regulation of local and long-range
1077 connections in mouse auditory cortex. *J Neurosci, 32*(5), 1643-1652.
1078 doi:10.1523/JNEUROSCI.4480-11.2012
1079 Xu, C., Liu, Q. Y., & Alkon, D. L. (2014). PKC activators enhance GABAergic neurotransmission and paired-
1080 pulse facilitation in hippocampal CA1 pyramidal neurons. *Neuroscience, 268*, 75-86.
1081 doi:10.1016/j.neuroscience.2014.03.008
1082 Zamir, O., & Charlton, M. P. (2006). Cholesterol and synaptic transmitter release at crayfish
1083 neuromuscular junctions. *J Physiol, 571*(Pt 1), 83-99. doi:10.1113/jphysiol.2005.098319
1084 Zhu, P. J., Chen, C. J., Mays, J., Stoica, L., & Costa-Mattioli, M. (2018). mTORC2, but not mTORC1, is
1085 required for hippocampal mGluR-LTD and associated behaviors. *Nat Neurosci, 21*(6), 799-802.
1086 doi:10.1038/s41593-018-0156-7
1087 Zoghbi, H. Y., & Bear, M. F. (2012). Synaptic dysfunction in neurodevelopmental disorders associated
1088 with autism and intellectual disabilities. *Cold Spring Harb Perspect Biol, 4*(3).
1089 doi:10.1101/cshperspect.a009886

1090